Electronic Supplementary Information (ESI)

Towards molecularly imprinted polymers that respond to and capture phosphorylated tyrosine epitopes using fluorescent bis-urea and bis-imidazolium receptors

Evgeniia Kislenko,[a] Anıl İncel,[b] Kornelia Gawlitza,[a] Börje Sellergren,[b] and Knut Rurack*[a]

[a]Chemical and Optical Sensing Division, Bundesanstalt für Materialforschung und –prüfung (BAM), Richard-Willstätter-Str. 11, D-12489 Berlin, Germany. E-mail: knut.rurack@bam.de
[b]Department of Biomedical Sciences, Faculty of Health and Society, Malmö University, SE-20506 Malmö, Sweden.

Contents

S1. Reagents, instruments, syntheses, methods

Reagents. All solvents were purchased from Chemsolute and used as received, unless stated otherwise. Deuterated dimethyl sulfoxide and tetrahydrofuran were purchased from Sigma-Aldrich. Spectroscopic chloroform, acetonitrile and ethanol were obtained from Merck. Anhydrous tetrahydrofuran, toluene and chloroform were received from Acros Organics and anhydrous dichloromethane from Carlo Erba. Acetonitrile (≥99.8% for HPLC) for equilibrium batch rebinding studies was received from VWR Chemicals. Milli-Q water was prepared via a Milli-Q water purification system from Millipore.

All chemicals were purchased from Sigma-Aldrich in the highest quality available, unless stated otherwise. Peptides Fmoc-Y-pY-G-OMe (95.46%), Fmoc-Y-Y-G-OMe (98.33%), GADDSYpYTAR (95.53%), GADDSpYpYTAR (96.16%) and GADDSYYTAR (95.13%) were purchased from LifeTein LLC and stored below –10 °C. L-tyrosine ethyl ester hydrochloride (99%), *N,N*-diisopropylethylamine (99%) and divinylbenzene (DVB-80, 80%, contains 1000 ppm 4-tert-butylcatechol as inhibitor) were purchased from Alfa Aesar. Ammonia (32% in water) and tetraethyl orthosilicate were received from Merck. 2,6-Di-tert-butyl-4-methylphenol (BHT, 99%) was purchased from Fluka. *N*-(9-Fluorenylmethoxycarbonyloxy)succinimide, (Fmoc-OSu, 98%) was obtained from J&K. 4-Cyano-4-(phenylcarbonothioylthio)pentanoic acid (CPDB, 97%) was purchased from ABCR. 2,2'-Azobis(2,4-dimethylvaleronitrile) V-65B (ABDV) was purchased from Wako Chemicals. Perchloric acid (60%) was obtained from Ferak Berlin. Potassium hydroxide was received from Fisher Scientific. Hydrochloric acid (≥37%), sodium chloride, sodium bicarbonate and pH buffer solutions with pH 4.01, 7.01 were purchased from Chemsolute. pH buffer with pH 9.00 was received from Metrohm. Trifluoroacetic acid, TFA (99%) was received from VWR Chemicals. Hydrochloric acid (≥37%) for equilibrium batch rebinding studies was received from Acros Organics.

Inhibitor removers: replacement packing for removing hydroquinone and monomethyl ether hydroquinone and replacement packing for removing tert-butylcatechol, were purchased from Sigma-Aldrich.

The aqueous buffers at different pH (1,3,5,7.4, 9.2) were prepared as follows. pH1 – Millipore water adjusted to pH 1 with 0.1 M HCl; pH 2 and 5: sodium citrate buffer (0.1M sodium citrate/citric acid); pH 7.4: sodium phosphate buffer (0.1 M); pH9.2: sodium carbonate (0.1M)

Instruments. ^{1}H, ^{13}C, ^{19}F and ^{31}P nuclear magnetic resonance spectra were acquired at 400 MHz on a Mercury 400 NMR spectrometer (Varian) in deuterated dimethyl sulfoxide (DMSO-d_6) using residual proton signals as standard (^{1}H: δ(DMSO-d_6 = 2.50 ppm), (^{13}C: δ(DMSO-d_6 = 39.52 ppm) and in deuterated tetrahydrofuran (THF-d_8, using residual proton signals as standard (^{1}H: δ(THF-d_8 = 3.58, 1.72 ppm), (^{13}C: δ(THF-d_8 = 67.21, 25.31 ppm). Chemical shifts are represented in δ (ppm).

Ultrahigh-performance liquid chromatography electrospray ionisation mass spectrometry (UPLC-ESI-MS) was performed on an Acquity UPLC (Waters) with an LCT Premier XE time-of-flight mass detector (Waters). Chromatographic separations were performed with a gradient of acetonitrile in water from 60 to 95% with 0.1% formic acid over 5 min with a constant flow rate of 0.6 ml min^{-1}.

Chromatographic separation with an automatic column was performed on a CombiFlash NextGen flash chromatography system (Teledyne ISCO) using a RediSep Rf Reversed-phase C18 (40–50 g) column (Teledyne ISCO). The chromatogram was monitored UV-spectrophotometrically at two wavelengths: 214 and 290 nm.

Absorption spectra and spectrophotometric titrations were acquired with a Specord 210 Plus spectrometer (Analytik Jena). Fluorescence emission and excitation spectra were measured with a FluoroMax 4 spectrofluorometer (HORIBA Scientific).

pH measurements were performed using a digital pH meter pH lab 827 (Metrohm) equipped with a glass electrode Biotrode (Metrohm).

Transmission electron microscopy (TEM) images were registered with a Talos F200S scanning/transmission electron microscope (Thermo Fisher Scientific).

Thermogravimetric analysis (TGA) was performed on a STA7200 thermobalance (Hitachi High-Tech Analytical Science); for each case, the sample was heated from 25 °C to 600 °C with a ramp of 10 °C min^{-1} in a nitrogen flow of 200 ml min^{-1} and from 600 °C to 1000 °C with a ramp of 10 °C min^{-1} in a synthetic airflow of 200 ml min^{-1}.

Elemental composition of bis-imidazolium salts was determined using a FlashEA 1112 Organic Elemental Analyzer (Thermo Fisher Scientific). Elemental composition of the functionalised silica core particles was determined using a Carbon/Sulfur Analyzer CS-800 (Eltra).

Equilibrium batch rebinding studies were performed on an Alliance 2695 HPLC (Waters) with a photodiode array detector 2996 (Waters) using Prodigy 5 µm ODS-3 100 Å 150 × 4.6 mm^2 C18 column (Phenomenex). Chromatographic separations were performed using a gradient of acetonitrile in water from 5 to 20% with 0.1% TFA over 10 min with an isocratic flow rate of 1.5 ml min^{-1}. The chromatogram was monitored UV-spectrophotometrically at wavelength of 210 nm.

Syntheses. The syntheses of the cross-linkers and protected amino acid derivatives are described in the following. The respective NMR spectra are included at the end of the ESI.

Preparation of 1,1'-[2,6-pyridinylbis(methylene)-bis[3-vinyl]-1H-imidazolium dibromide, bIm-Br. Compound **bIm-Br** was prepared according to a previously published protocol with slight alterations (Scheme S1).[1] 2,6-Bis-(bromomethyl) pyridine (500 mg, 1.89 mmol) and BHT (8.9 mg, 0.04 mmol), which was added to prevent a polymerisation, were dissolved in acetonitrile (25 ml) in a 50 ml round-bottom flask. *N*-Vinylimidazole (0.35 ml, 3.78 mmol) was added and the reaction solution was refluxed overnight at 95 °C. After 18 h the reaction mixture was cooled to room temperature and the solvent was evaporated. The product **bIm-Br** was recrystallised from ethanol by adding diethyl ether (656.4 mg, 79% yield). ^{1}H NMR (400 MHz, DMSO-d_6): δ = 9.62 (t, J=1.5 Hz, 2H), 8.21 (t, J=1.8 Hz, 2H), 7.99 (t, J = 7.7 Hz, 1H), 7.84 (t, J = 1.7 Hz, 2H), 7.55 (d, J = 7.7 Hz, 2H), 7.36 (dd, J = 15.7, 8.8 Hz, 2H), 5.99 (dd, J = 15.6, 2.5 Hz, 2H), 5.63 (s, 4H), 5.45 (dd, J = 8.7, 2.5 Hz, 2H) ppm. ^{13}C NMR (400 MHz, DMSO-d_6): δ = 152.99, 138.49, 136.09, 128.72, 124.12, 122.12, 118.66, 108.91 52.72 ppm. HRMS-TOF (ESI+): m/z calculated for $[M]^+$ 450.9996, 372.0813 and 293.1629, found 372.0836 and 293.1631. Elemental analysis: calculated for C, 45.06%, H, 4.23%, N, 15.45%; found C, 44.20%, H, 4.50%, N, 15.02%.

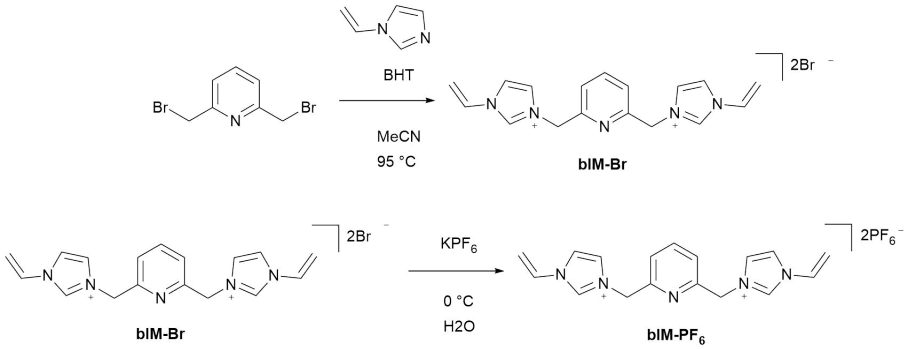

Scheme S1. Synthesis of functional cross-linkers **bIm-Br** and **bIm-PF_6**.

Preparation of 1,1'-[2,6-pyridinylbis(methylene)-bis[3-vinyl]-1H-imidazolium dihexafluoro-phosphate, bIm-PF6. Compound **bIm-PF_6** was prepared according to an adapted version of a previously published protocol (Scheme S1).[2] Potassium hexafluorophosphate (412.7 mg, 2.22 mmol)

was dissolved in distilled water (6 ml) in a 50 ml round-bottom flask and cooled down to 0 °C with an ice bath. **bIm-Br** (100 mg, 0.22 mmol) was dissolved in distilled water (2 ml) and added dropwise to the solution in 1 min. The resulting suspension was stirred for 10 min and filtered. The solid was washed with cold water (3× 10 ml) and dried in a vacuum oven overnight to obtain **bIm-PF_6** as a white powder (54.3 mg, 42% yield). ^{1}H NMR (400 MHz, DMSO-d_6): δ = 9.42 (t, J=1.4 Hz, 2H), 8.13 (t, J=1.8 Hz, 2H), 7.98 (t, J = 7.7 Hz, 1H), 7.77 (t, J = 1.7 Hz, 2H), 7.52 (d, J = 7.7 Hz, 2H), 7.28 (dd, J = 15.6, 8.8 Hz, 2H), 5.94 (dd, J = 15.6, 2.5 Hz, 2H), 5.57 (s, 4H), 5.45 (dd, J = 8.7, 2.5 Hz, 2H) ppm. ^{13}C NMR (400 MHz, DMSO-d_6): δ = 153.09, 138.81, 136.10, 128.69, 124.06, 122.15, 118.70, 108.95, 52.79 ppm. ^{19}F NMR (400 MHz, DMSO-d_6): δ = -69.24, -71.13 ppm. HRMS-TOF (ESI+): m/z calculated for $[M]^+$ 583.0913, 438.1271 and 293.1629, found 438.1261 and 293.1609. Elemental analysis: calculated for C, 35.01%, H, 3.28%, N, 12.0 1%; found C, 33.47%, H, 2.94%, N, 11.02%.

Preparation of (((phenazine-2,3-diylbis(azanediyl))bis(carbonyl))bis(azanediyl))-bis(ethane-2,1-diyl) bis(2-methylacrylate), fCL. Compound **fCL** was prepared according to a refined version of our previously published protocol (Scheme S2).[3] Under an argon atmosphere, 2,3-diaminophenazine (1.00 g, 4.28 mmol) and BHT (0.095 g, 0.43 mmol) were added into a 100 mL round-bottom flask, which was previously dried under vacuum with a heat gun. Anhydrous tetrahydrofuran (35 ml) was added to the flask. Half of the 2-isocyanatoethyl methacrylate (1.23 ml, 8.56 mmol) was added while stirring continuously under argon and the reaction was heated at 60 °C for 2 h before the second half of 2-isocyanatoethyl methacrylate (1.23 ml, 8.56 mmol) was added while continuing stirring under argon whereafter the reaction was left at 60 °C for another 20 h. The reaction mixture was cooled to room temperature and the solvent was evaporated, then the reaction mixture was purified by silica gel column chromatography using dichloromethane/methanol (90:1 → 10:1 v/v) as eluent to obtain fCL as a bright yellow solid (0.25 g, 11% yield). ^{1}H NMR (400 MHz, DMSO-d_6): δ = 8.48 (s, 2H), 8.40 (s, 2H), 8.13 (ddd, J = 12.7, 3.9, 1.3 Hz, 2H), 7.82 (ddd, J = 12.8, 3.7, 1.0 Hz, 2H), 7.01 (t, J = 5.7 Hz, 2H), 6.11 (dq, J = 1.7, 1.0 Hz, 2H), 5.71 (quintet, J = 1.6, 1.6 Hz, 2H), 4.21 (t, J = 5.6 Hz, 4H), 3.49 (q, J = 5.6, 5.5 Hz, 4H), 1.92 (dd, J = 1.5, 1.0 Hz, 6H) ppm. ^{13}C NMR (400 MHz, DMSO-d_6): δ = 166.59, 155.37, 142.11, 141.10, 136.43, 135.81, 129.53, 128.89, 126.01, 116.70, 63.82, 38.44, 18.00 ppm. HRMS-TOF (ESI^-): m/z calculated for $[M-H]^-$ 519.1992, found 519.1913.

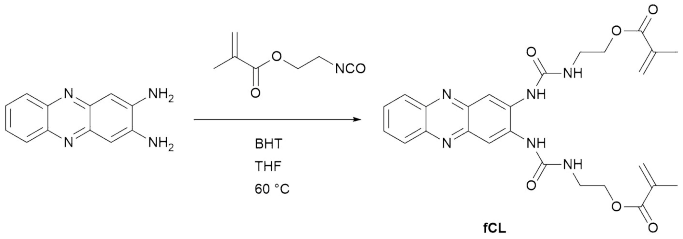

Scheme S2. Synthesis of fluorescent cross-linker **fCL**.

Preparation of N-(9-fluorenylmethyloxycarbonyl)-tyrosine ethyl ester, Fmoc-Y-OEt. Compound Fmoc-Y-OEt was prepared according to a previously published protocol with some alterations (Scheme S3).[4] *L*-Tyrosine ethyl ester hydrochloride (500 mg, 0.81 mmol) was suspended in dry dichloromethane (20 ml) in a 50 ml round-bottom flask and sonicated for 10 min. The suspension was degassed with argon for 5 min under stirring. Fmoc-OSu (278.8 mg, 0.81 mmol) was added and the reaction solution was stirred for 15 min at room temperature. The reaction mixture was cooled down to 0 °C with an ice bath. *N*,*N*-Diisopropylethylamine (DIPEA) (0.14 ml, 0.81 mmol) was added dropwise. After 5 min the ice bath was removed, and the resulting solution was stirred under argon for 16 h. The solvent was evaporated, and the reaction mixture was dissolved in ethyl acetate (40 ml) and washed with 1 M hydrochloric acid (2× 40 ml), saturated solution of sodium bicarbonate (2× 40 ml), water (2× 40 ml) and brine (2× 40 ml). The combined organic phases were dried over anhydrous magnesium sulfate. The reaction mixture was concentrated under reduced pressure and purified by a reverse-phase silica gel column chromatography using an automatic column with water/acetonitrile (100:0 → 40:60 v/v

for 27 min with a constant flow rate of 30 ml min^{-1}) as eluent to obtain Fmoc-Y-OEt as a white solid (635 mg, 73% yield). ^{1}H NMR (400 MHz, THF-d_8): δ = 8.04 (s, 1H), 7.76 (d, J = 7.5 Hz, 2H), 7.60 (t, J = 7.1 Hz, 2H), 7.33 (t, J = 7.4 Hz, 2H), 7.25 (td, J = 7.4, 1.1 Hz, 2H), 6.98-6.96 (m, 2H), 6.77 (d, J = 8.4 Hz, 1H), 6.63 (d, J = 8.4 Hz, 2H), 4.43 (dd, J = 14.1, 8.0 Hz, 1H), 4.28 (ddd, J = 23.5, 10.4, 7.2 Hz, 2H), 4.18 (t, J = 7.0 Hz, 1H), 4.09 (q, J = 7.1 Hz, 2H), 2.99 (dd, J = 13.8, 5.8 Hz, 1H), 2.86 (dd, J = 13.8, 7.9 Hz, 1H), 1.18 (t, J = 7.1 Hz, 3H) ppm. ^{13}C NMR (400 MHz, THF-d_8): δ = 172.36, 157.38, 156.49, 145.19, 145.16, 142.12, 142.11, 130.84, 128.21, 128.11, 127.58, 125.93, 125.87, 120.41, 115.75, 66.99, 61.17, 56.45, 48.16, 37.91, 14.36 ppm.

Preparation of N-(9-fluorenylmethyloxycarbonyl)-O-phosphotyrosine ethyl ester, Fmoc-pY-OEt. Compound Fmoc-pY-OEt was prepared according to a previously published protocol with some alterations (Scheme S3).[4] Fmoc-Y-OEt (125 mg, 0.29 mmol) was dissolved in dry dichloromethane (15 ml) in a 50 ml round-bottom flask and degassed with argon for 10 min under stirring. The reaction mixture was cooled down to –10 °C with an ice/salt bath. Phosphoryl chloride (0.055 ml, 0.58 mmol) was added dropwise followed by DIPEA (0.061 ml, 0.35 mmol) in dry dichloromethane (1.5 ml). After 15 min the cooling bath was removed, and the resulting solution was stirred under argon for 2 h. The reaction mixture was washed with 1 M hydrochloric acid (2× 10 ml) and brine (2× 10 ml) and both aqueous phases were combined and washed with dichloromethane (2× 10 ml). The combined organic phases were dried over anhydrous magnesium sulfate. The reaction mixture was concentrated under reduced pressure. The solid residue was dissolved in acetone (10 ml) and then distilled water (10 ml) was added under stirring. The reaction was left for 2 h under stirring at room temperature. The solvents were evaporated and the reaction mixture was purified by a reverse-phase silica gel column chromatography using an automatic column with water/acetonitrile (100:0 → 40:60 v/v for 25 min with a constant flow rate of 25 ml min^{-1}) as eluent to obtain Fmoc-pY-OEt as a white solid (71.4 mg, 48% yield). ^{1}H NMR (400 MHz, THF-d_8): δ = 7.76 (d, *J* = 7.5 Hz, 2H), 7.67-7.58 (m, 2H), 7.34 (t, *J* = 7.4 Hz, 2H), 7.26 (t, *J* = 7.4 Hz, 2H), 7.12 (q, *J* = 7.5 Hz, 4H), 6.91 (d, *J* = 8.5 Hz, 1H), 5.36 (bs, 4H), 4.44 (dd, *J* = 14.0, 7.9 Hz, 1H), 4.37-4.24 (m, 2H), 4.18 (t, *J* = 6.9 Hz, 1H), 4.09 (q, *J* = 7.1 Hz, 2H), 3.05 (dd, *J* = 13.8, 5.7 Hz, 1H), 2.93 (dd, *J* = 13.8, 8.0 Hz, 1H), 1.16 (t, *J* = 7.1 Hz, 3H) ppm. ^{13}C NMR (400 MHz, THF-d_8): δ = 172.17, 156.62, 151.66, 145.17, 145.04, 142.12, 133.75, 130.88, 128.17, 127.64, 125.84, 120.88, 120.43, 66.95, 61.35, 56.32, 48.14, 37.80, 14.37. ^{31}P NMR (400 MHz, THF-d_8): δ = -4.11 ppm.

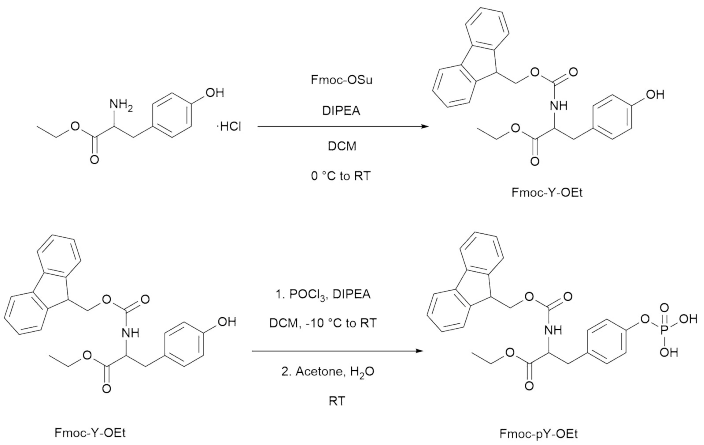

Scheme S3. Synthesis of Fmoc-Y-OEt and Fmoc-pY-OEt.

Preparation of tetrabutylammonium (TBA) and tetrahexylammonium (THA) salts of templates/analytes. The template was dissolved in an appropriate amount of acetonitrile to ensure complete dissolution after 15 min of sonication. Stochiometric amounts of tetrabutylammonium hydroxide 30–hydrate (TBA-OH) or tetrahexylammonium hydroxide (THA-OH, ~40% in water) were added and the mixtures were sonicated for an additional 10 min. The salts were concentrated under reduced pressure for 4 h in a vacuum concentrator to obtain transparent or semi-transparent solids.

The dried salts were used immediately or kept overnight in a desiccator or as a solution in an appropriate aprotic solvent in the freezer.

Synthesis of silica (SiO_2) particles grafted with reversible addition-fragmentation chain transfer (RAFT) agent.[5] The SiO_2 core particles were produced via a modified Stöber protocol using tetraethyl orthosilicate (TEOS) as a source of silica. Aqueous ammonia solution (32%, 20 ml) was mixed with absolute ethanol (65 ml) and Milli-Q water (115 ml) at 300 rpm in a 1000 ml Erlenmeyer flask. TEOS (18 ml) and absolute ethanol (182 ml) were briefly mixed in a 250 ml Erlenmeyer flask at 500 rpm and added to the ammonia solution at 300 rpm. After 18 h, the particles were washed with 96% ethanol (3× 100 ml) with centrifugation at 9000× g for 10 min in between the washing steps. The SiO_2 particles were dried overnight in a vacuum oven to obtain a white powder (5.58 g).

Amino-modified silica (NH_2-SiO_2) particles were synthesised by functionalisation with (3-aminopropyl)triethoxysilane (APTES). SiO_2 particles (1 g) were dispersed in anhydrous toluene (30 ml) in a 50 ml round-bottom flask by sonication. Dry toluene was chosen as a reaction medium to avoid APTES self-condensation[6] and to increase the reaction temperature which allows for higher hydrolytic stability of the produced amino functionalised (NH_2-SiO_2) particles.[7] The suspension was degassed for 15 min with argon. APTES (3 ml) was added and the reaction was refluxed at 120 °C under argon at 700 rpm. After 20 h, the particles were washed with 96% ethanol (2× 20 ml), 96% ethanol/Milli-Q water 1:1 v/v solution (2× 20 ml) and 96% ethanol (2× 20 ml) with centrifugation at 9000× g for 5 min in between the washing steps. The NH_2-SiO_2 particles were dried overnight in a vacuum oven to obtain a white powder (0.92 g).

RAFT-modified silica (RAFT-SiO_2) particles were synthesised using the RAFT agent CPDB. CPDB (0.25 g, 0.87 mmol) was dissolved in anhydrous tetrahydrofuran (5 ml) in a 10 ml glass vial and degassed for 10 min. The reaction mixture was cooled down to –78 °C using an acetone/liquid nitrogen bath. Ethyl chloroformate (0.083 ml, 0.87 mmol) and triethylamine (0.12 ml, 0.87 mmol) were added under argon and the reaction was left under stirring for 1 h. NH_2-SiO_2 particles (0.8 g) were placed in a 50 ml round-bottom flask and were well-dispersed by sonication in anhydrous tetrahydrofuran (4 ml). The particles were cooled down to –10 °C with an ice/salt bath and degassed for 10 min under stirring at 700 rpm. CPDB solution was transferred to the vial containing the particles via a cannula. 2 ml of anhydrous tetrahydrofuran was added additionally to the vial containing CPDB to ensure the transfer of all the activated RAFT agent. The suspension was mixed at room temperature at 700 rpm. After 20 h, the particles were precipitated using n-hexane (15 ml) and washed with tetrahydrofuran (10 ml), acetone (2× 10 ml) and again tetrahydrofuran (2× 10 ml) with centrifugation at 9000× g for 5 min in between the washing steps. The RAFT-SiO_2 particles were dried overnight in a vacuum oven to obtain a pink powder (0.76 g).

Synthesis of M1no, N1no, M1D and N1D core-shell polymer@SiO_2 particles for evaluation of the influence of bIm-PF_6 inclusion in the polymer shell on MIP and NIP behaviour. M1no, **N1no**, **M1D** and **N1D** were synthesised according to a synthetic procedure for **M1bIm** and **N1bIm**, using the amount of polymerisation components in Table S1.

Table S1. Amount of polymerisation components for **M1no**, **N1no**, **M1D** and **N1D** core-shell polymer@SiO_2 particles.

Sample	T[a], mg	fCL, mg	MAAm, mg	Monomer[b], µl	EGDMA, µl	ABDV, mg	$CHCl_3$, ml	RAFT-SiO_2, mg
M1no	1.01	0.55	1.83	–	20.6	2	2	20
N1no	–	0.55	1.83	–	20.6	2	2	20
M1D	1.01	0.55	1.83	0.094[b]	20.6	2	2	20
N1D	–	0.55	1.83	0.094[b]	20.6	2	2	20

[a]Template: Fmoc-Y-pY-G-OMe-TBA, [b]Monomer: DVB-80

Synthesis of M3bIm and N3bIm core-shell polymer@SiO2 particles. M3bIm and **N3bIm** were synthesised by increasing the amount of reaction components four-fold compared to **M1bIm** and **N1bIm**, respectively (Table S2).

Table S2. Amount of polymerisation components for **M3bIm** and **N3bIm** core-shell polymer@SiO_2 particles.

Sample	T[a], mg	fCL, mg	MAAm, mg	bIm-PF_6, mg	EGDMA, µl	ABDV, mg	$CHCl_3$, ml	RAFT-SiO_2, mg
M3bIm	4.04	2.2	7.32	1.24	82.4	8	8	80
N3bIm	–	2.2	7.32	1.24	82.4	8	8	80

[a]Template: Fmoc-Y-pY-G-OMe-TBA

NMR studies of counterion exchange. The ^{1}H NMR spectra show an up-field shift of the imidazolium protons upon counterion exchange from **bIm-Br** to **bIm-PF_6** (Fig. S1). The peak from the H2 protons is shifted from 9.62 to 9.42 ppm while smaller shifts were found for the H4 and H5 protons, from 8.21 to 8.13 ppm and from 7.84 to 7.77 ppm, respectively (Fig. S1). The shifts correspond well with previously reported data for structurally similar bis-imidazolium salts.[8] Whereas the imidazolium proton at the C2 position in 1,3-disubstituted imidazolium was reported to be highly sensitive to the electronic environment, H4 and H5 are less sensitive, with the strength of the interaction between H2 proton and the counterion being proportional to the NMR shift.[9] Hexafluorophosphate, a larger and more polarisable anion compared to bromide, interacts only weakly with the proton,[10] and mostly participates in anion-π interaction with the imidazolium ring system,[11] causing the shift of the NMR peaks and proving the successful anion exchange.

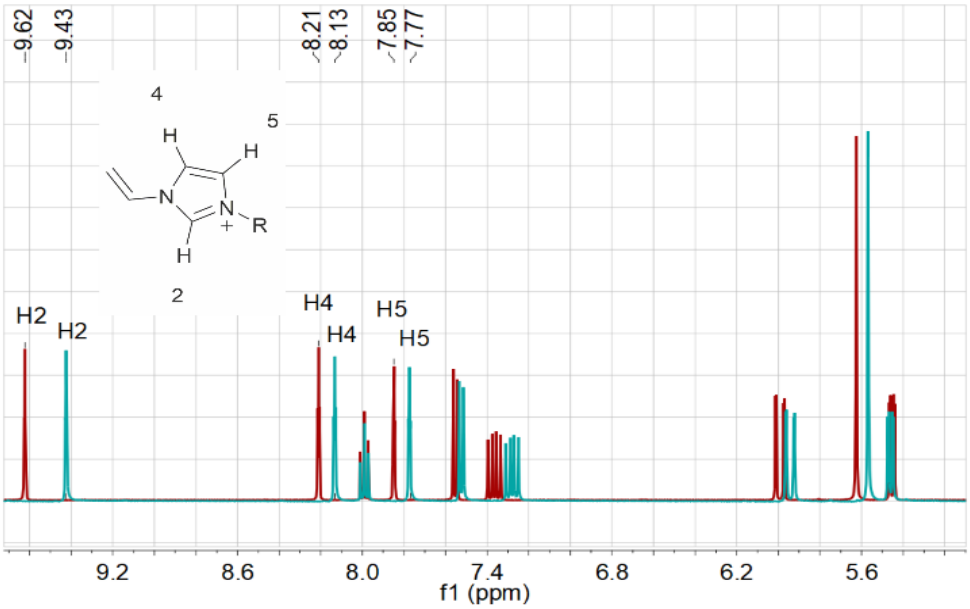

Fig. S1. ^{1}H NMR spectra in DMSO-d_6 at 400 MHz; **bIm-Br** – red line, **bIm-PF_6** – cyan line.

Particle characterisation. The size of the SiO_2 core particles and shell thickness for MIP and NIP core-shell polymer@SiO_2 particles was measured using transmission electron microscopy (TEM) using particle solutions of 0.25 mg ml^{-1} in absolute ethanol and placing 9 µL on a copper grid with a carbon film. Statistical analysis was conducted with the free software ImageJ 1.51j8[12] and Origin 2018. Thermogravimetric analysis (TGA) and the changes in zeta potential for the particles after each functionalisation step were used to confirm a successful functionalisation and grafting. Elemental

analysis of the sulfur content in the samples was used to quantify the number of RAFT groups attached to the surface of the RAFT-SiO_2 particles.

Pre-polymerisation studies. To evaluate the photophysical properties and binding equilibrium of the reaction mixture at polymerisation concentrations, the pre-polymerisation mixture was measured in a customised setup using thin quartz cuvettes with an optical path of ~100 µm and front-face detection in the fluorometer while employing 14 µl of solution. This approach accounts for the high concentration of fluorophore that is present in the polymerisation mixture and avoids reabsorption or inner-filter effects. Wavelength settings for fluorescence emission were listed above and fluorescence excitation spectra were recorded with observation wavelengths of 490 or 495 nm. Slits were set to keep the signal intensity below 10^6 counts per second. The concentration of the components is summarized in Table S3.

Table S3. Pre-polymerisation components concentration in chloroform.

Compound	Eq.	c, mM
fCL	1	1.11
bIm-Br or **bIm-PF_6**	0.1	0.11
bIm-Br or **bIm-PF_6**	1	1.11
HPPA-TBA	1	1.11
PPA-TBA_2	1	1.11

Titrations of fCL at dilute conditions. To evaluate the fluorescence response of the fluorescent cross-linker **fCL** upon analyte addition, diluted solutions of **fCL** (ca. 6.5 µM) in chloroform with an absorption of ca. 0.1 at the absorption maximum were placed in a 10×10 mm quartz cuvette. 1 mM of freshly prepared analyte stock solution was used for the titration. The excitation wavelength used for fluorescence measurements was 385 nm and for recording fluorescence excitation spectra, emission wavelengths of 490 or 650 nm were used. Slits were set to keep the signal intensity below 10^6 counts per second.

NMR binding studies. To evaluate the affinity of the phosphate group to **bIm-PF_6**, freshly prepared mono-deprotonated tetrabutylammonium salt of phenylphosphoric acid (HPPA-TBA) was used. The increasing amount of analyte (0–10 eq.) in DMSO-d_6 was added to the solution of **bIm-PF_6** in DMSO-d_6 (5 mM) in oven-dried NMR tubes. ^{1}H NMR spectra were recorded for each sample.

S2. Pre-polymerisation studies—additional results

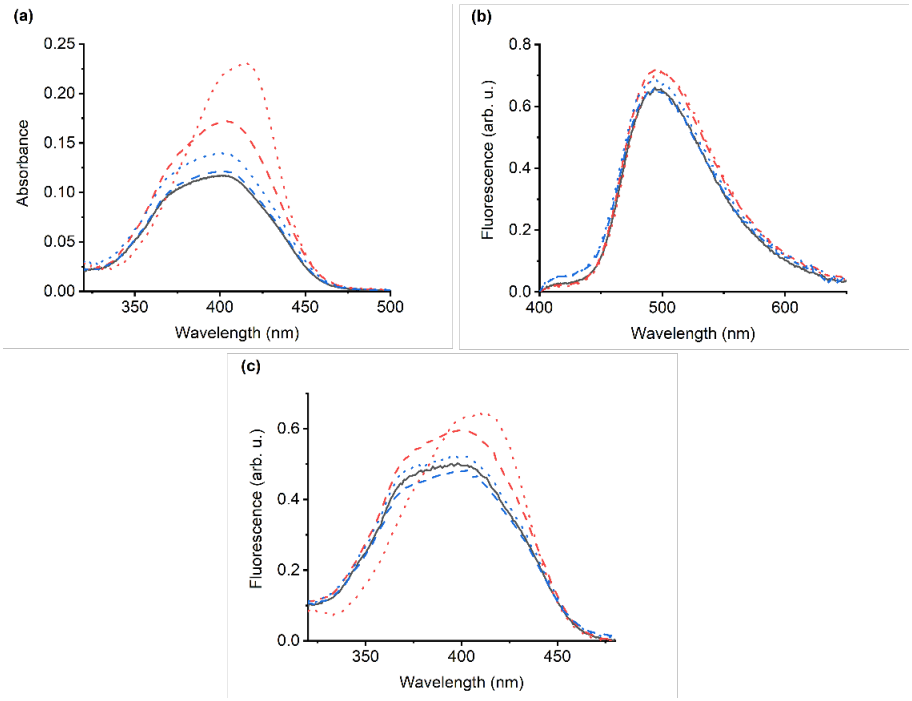

Fig. S2. Absorption (a), fluorescence emission (λ_{exc} = 385 nm) (b) and excitation (λ_{em} = 495 nm) (c) spectra of prepolymerisation mixture of **fCL** (1.11 mM) in chloroform with 0.1 eq. and 1 eq. of **bIm-Br** and **bIm-PF$_6$** in chloroform; **fCL –** black line, **fCL** and 0.1 eq. of **bIm-Br** – dashed red line, **fCL** and 1 eq. of **bIm-Br** – dotted red line, **fCL** and 0.1 eq. of **bIm-PF$_6$** – dashed blue line and **fCL** and 1 eq. of **bIm-PF$_6$** – dotted blue line.

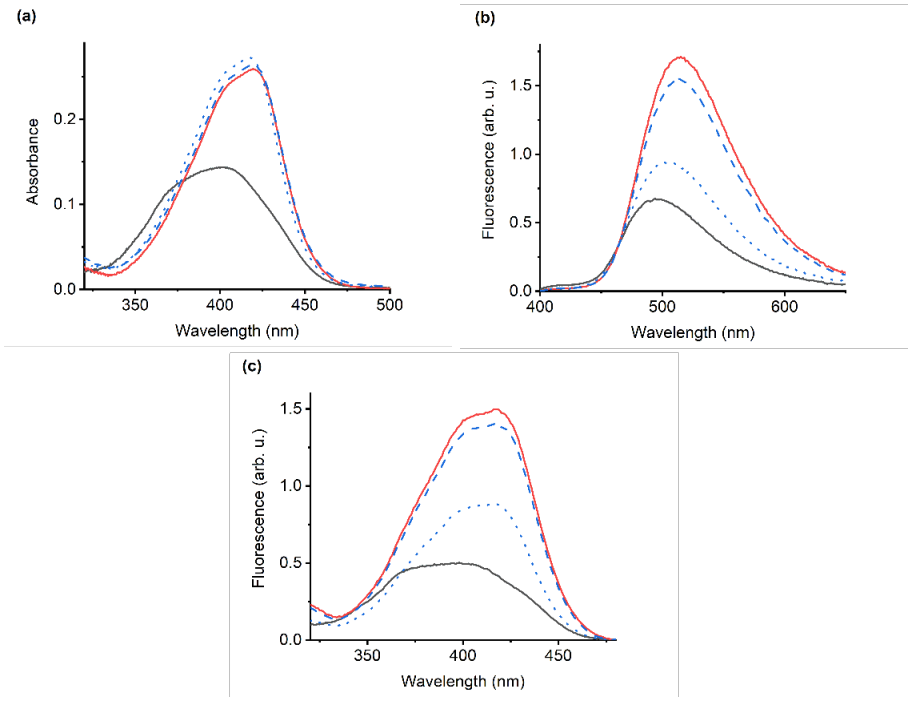

Fig. S3. Absorption (a), fluorescence emission (λ_{exc} = 385 nm) (b) and excitation (λ_{em} = 495 nm) (c) spectra of prepolymerisation mixture of **fCL** (1.11 mM) in chloroform with 1 eq. of HPPA-TBA as well as 0.1 eq. and 1 eq. of **bIm-Br** in chloroform; **fCL –** black line, **fCL** and 1 eq. of HPPA-TBA – red line, **fCL**, 1 eq. of HPPA-TBA and 0.1 eq. of **bIm-Br** – dashed blue line and **fCL**, 1 eq. of HPPA-TBA and 1 eq. of **bIm-Br** – dotted blue line.

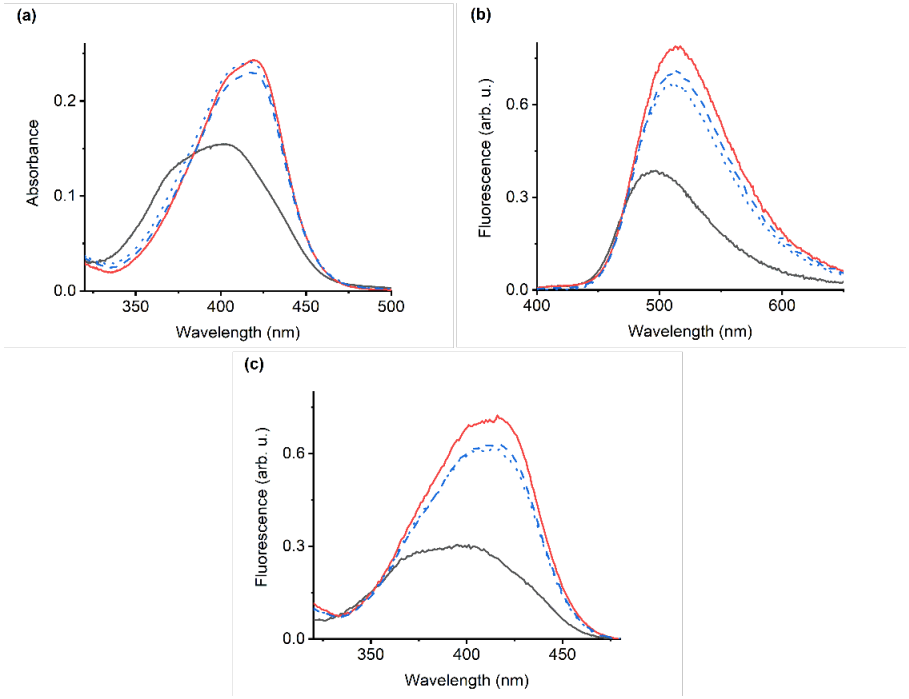

Fig. S4. Absorption (a), fluorescence emission (λ_{exc} = 385 nm) (b) and excitation (λ_{em} = 495 nm) (c) spectra of prepolymerisation mixture of **fCL** (1.11 mM) in chloroform with 1 eq. of HPPA-TBA as well as 0.1 eq. and 1 eq. of **bIm-PF$_6$** in chloroform; **fCL –** black line, **fCL** and 1 eq. of HPPA-TBA – red line, **fCL**, 1 eq. of HPPA-TBA and 0.1 eq. of **bIm-PF$_6$** – dashed blue line and **fCL**, 1 eq. of HPPA-TBA and 1 eq. of **bIm-PF$_6$** – dotted blue line.

To assess whether the dicationic **bIm** influences the behaviour of Br^- and PF_6^- in the reported studies, the influence of the TBA-Br and TBA-PF_6 on the spectroscopic properties of fCL was investigated. As a comparison of Fig. S5 and Fig. S2 shows, the behaviour of the TBA and the **bIm** salts is very similar.

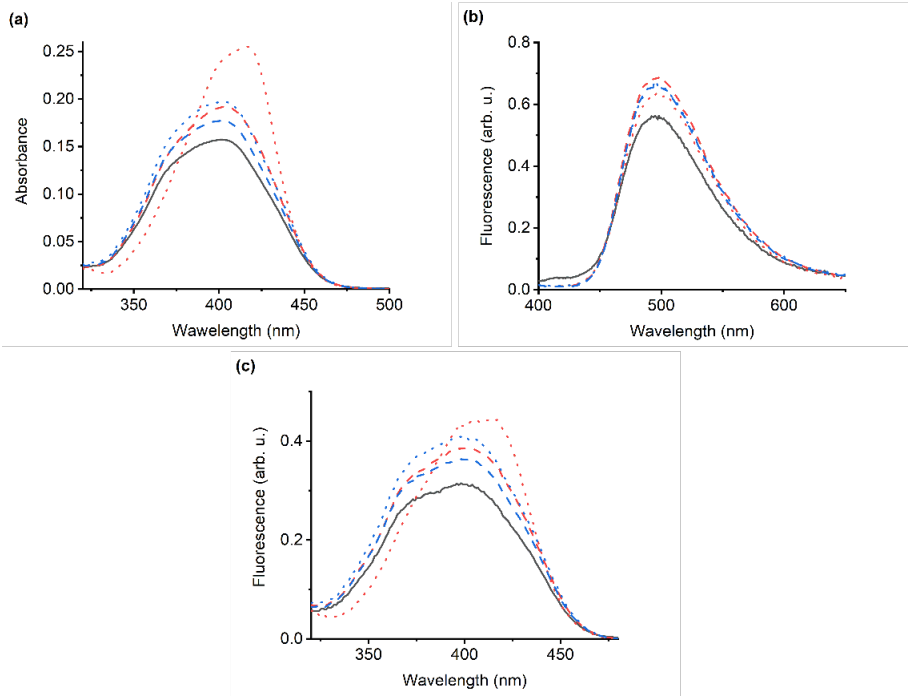

Fig. S5. Absorption (a), fluorescence emission (λ_{exc} = 385 nm) (b) and excitation (λ_{em} = 495 nm) (c) spectra of prepolymerisation mixture of **fCL** (1.11 mM) in chloroform with 0.1 eq. and 1 eq. of TBA-Br and TBA-PF_6 in chloroform; **fCL –** black line, **fCL** and 0.1 eq. of TBA-Br – dashed red line, **fCL** and 1 eq. of TBA-Br – dotted red line, **fCL** and 0.1 eq. of TBA-PF_6 – dashed blue line and **fCL** and 1 eq. of TBA-PF_6 – dotted blue line.

S3. Quantum chemical calculations

Quantum chemical calculations employing density functional theory (DFT) with the B3LYP functional and the 6-31G basis set as implemented in Gaussian 16W[13] were performed to better illustrate the binding geometries in the various possible complexes. The monoanion of phenylphosphoric acid, $HPPA^-$, is bound in the cleft-like arrangement of the two urea groups of **fCL** through three strong and one weaker hydrogen bond (Fig. S6a), the two urea groups of **fCL** being largely coplanar with an average deviation from planarity of the four urea protons of 0.027 Å in $[\mathbf{fCL}\subset HPPA]^-$ (Fig. S7a). If both polymerisable groups are covalently incorporated into a network the cleft-like arrangement is expected to be retained.

The bromide complex of **fCL** has a very similar geometry, the longer bond lengths arising from the larger ionic radius of Br^- (Fig. S6b). Also for such a complex, the arrangement of both binding sites in the cleft is coplanar (Fig. S7b). A possible complex conformation as shown in Fig. S8a is energetically less favored. As **fCL** possesses two urea binding sites and Br^- is a monoatomic small anion, in principle, one molecule of **fCL** can bind two Br^-. In such a scenario, the energetically preferred situation would be the one as shown in Fig. S6c, i.e., one Br^- would be bound through three H bonds and one only weakly through a single H bond. Accordingly, the arrangement of the two urea sites would be largely distorted (Fig. S7c). The possible complex conformation shown in Fig. S8b is energetically less favored.

Finally, in theory, a complex is also formed in vacuo between **fCL** and PF_6^-. However, despite the cleft being retained, the planarity of the two urea groups is further distorted, the average deviation from planarity of the four urea protons amounting to 0.240 Å (Fig. S7d). Furthermore, it has to be noted that if the angle between the two urea moieties is increased, the distance between the two polymerisable groups at the distant ends is growing proportionally, which has to be considered when aiming to fix the fluorescent crosslinker in the polymer network. Thus, based on geometrical and electronic (charge density) considerations the complex between **fCL** and a single Br^- is the most critical competitor to the desired complexes between **fCL** and template.

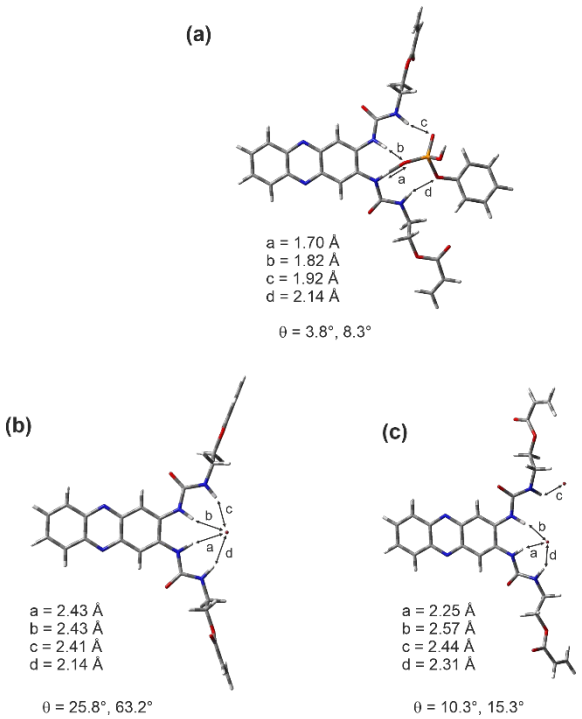

Fig. S6. Optimised ground-state geometries of isolated complexes of $[\mathbf{fCL}\subset HPPA]^-$ (a), $[\mathbf{fCL}\subset Br]^-$ (b) and $[\mathbf{fCL}\subset Br_2]^{2-}$ (c) with the four most prominent hydrogen bond lengths indicated.

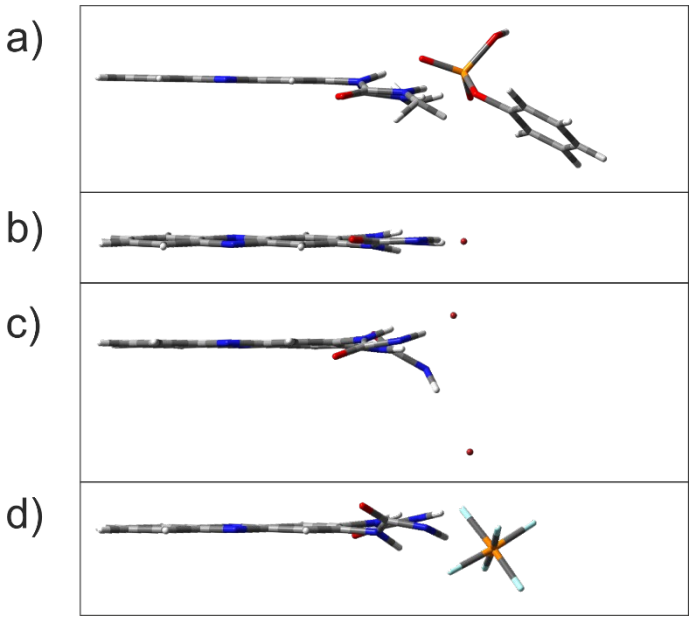

Fig. S7. Side (in-plane) views of urea$_1$-phenazine-urea$_2$ fragments and anion guests of optimised ground-state geometries of isolated complexes of [**fCL**⊂HPPA]$^-$ (a), [**fCL**⊂Br]$^-$ (b), [**fCL**⊂Br$_2$]$^{2-}$ (c) and [**fCL**⊂PF$_6$]$^-$ (d).

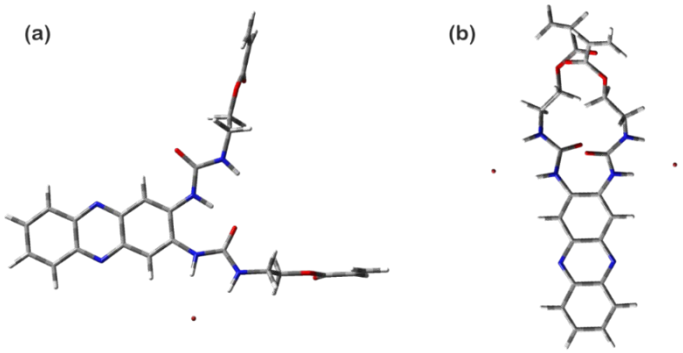

Fig. S8. Optimised ground-state geometries of alternative conformations of isolated complexes of [**fCL**⊂Br]$^-$ (a) and [**fCL**⊂Br$_2$]$^{2-}$ (b).

S4. Binding constants in chloroform

To calculate the strength of interaction between **fCL** (3.14 μM) and mono-deprotonated tetrabutylammonium salt of tripeptide Fmoc-pY-Y-G-OMe (Fmoc-Y-pY-G-OMe-TBA) in the diluted solution in chloroform increasing concentrations of analyte (0–63.1 eq.) were added until the saturation point was reached. The absorption data (Fig. 3a) were fitted using a 1:1 (host:guest) non-linear binding model with BindFit software.[14-16] The binding constant was calculated as K_a = 60695 ± 1142 M^{-1} (Fig. S9).

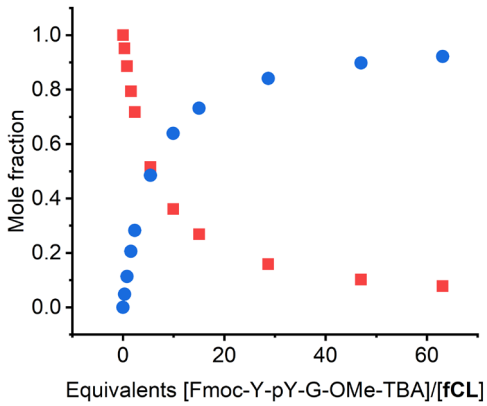

Fig. S9. Relative species concentration during the titration of 3.14 μM of **fCL** in chloroform with an increasing amount of Fmoc-Y-pY-G-OMe-TBA (0–63.1 eq.) in chloroform as derived from BindFit fitting; **fCL** – red ■, complex – blue ●.

S5. TEM images analysis of particles

TEM images of core SiO_2 particles and core-shell polymer@SiO_2 particles (Fig. S10) were analysed using the free software ImageJ 1.51j8[12] and Origin 2018. To measure the diameter of the particles the scale bar from the images was used as a reference. The original TEM images were converted to 8-bit (256 shades of gray) images first. To define the particles a binary contrast enhancement procedure such as thresholding was used. Using the ImageJ tool "Analyze particles" the size of particles was estimated. The shell thickness for MIP and NIP particles was measured in 8-bit images.

To perform the statistical analysis 85 points on average were measured. To calculate the mean size and shell thickness and their standard deviation the measured data points were fitted with a normal Gaussian distribution in Origin 2018. Polydispersity index (PDI) can be used to evaluate the size homogeneity of particles diameter or shell thickness, with PDI values from 0 to 0.04 indicating the highly monodisperse quantity.[17] PDI was calculated using Equation S1, where σ is the standard deviation and x_c is the mean from the Gaussian fit (Fig. S11 and Fig. S12).[17] The results are summarised in Table S4.

Equation S1. PDI calculation.

$$PDI = \left(\frac{\sigma}{x_c}\right)^2$$

Table S4. Size and shell thickness of SiO_2 core and MIP and NIP core-shell polymer@SiO_2 particles from TEM.

Sample	Diameter, nm	Shell thickness, nm
SiO_2	318.1 ± 24.0	n.a.
M1bIm	320.6 ± 24.6	3.2 ± 1.4
N1bIm	325.3 ± 12.7	4.0 ± 1.2
M2bIm	323.4 ± 88.0	7.8 ± 2.5
N2bIm	326.0 ± 14.7	8.2 ± 2.1
M3bIm	326.4 ± 46.2	4.6 ± 1.4
N3bIm	329.7 ± 27.9	5.3 ± 2.1

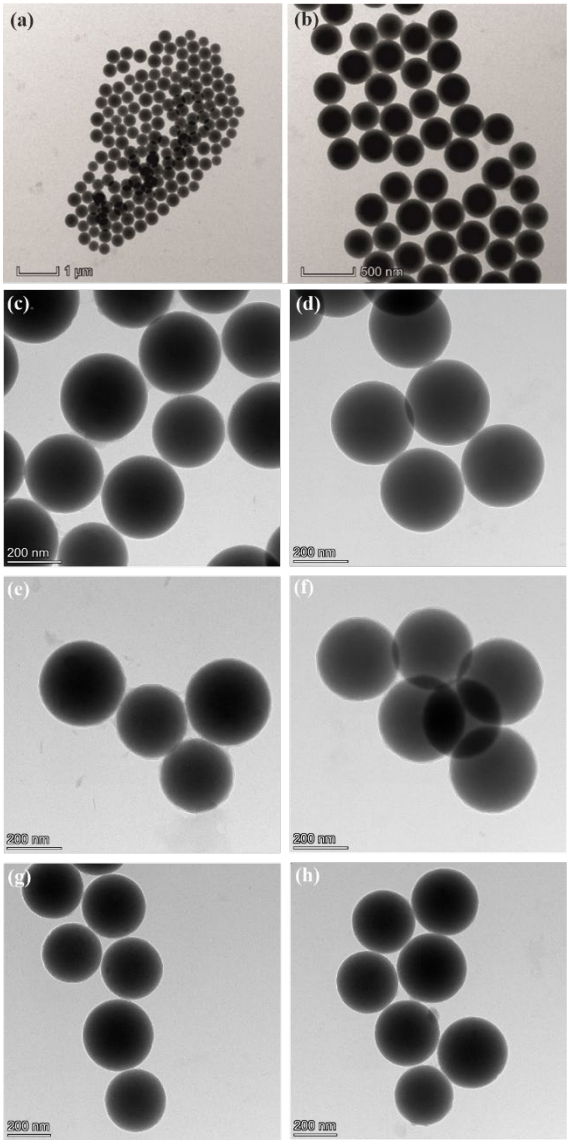

Fig. S10. TEM images of SiO_2 core (a and b), **M1bIM** (c), **N1bIM** (d), **M2bIm** (e), **N2bIm** (f), **M3bIm** (g) and **N3bIm** (h) core-shell polymer@SiO_2 particles.

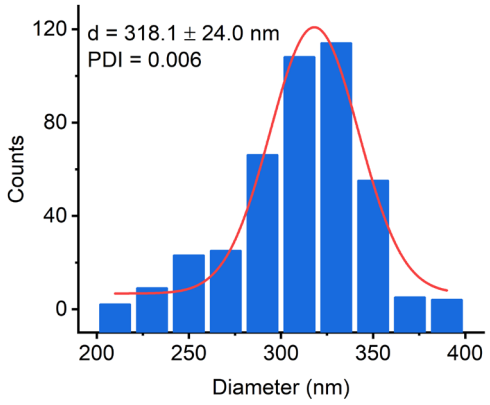

Fig. S11. Particles size distribution and Gaussian fit for core SiO_2 particles; core SiO_2 particles size distribution – blue bars, Gaussian fit of distribution – red line.

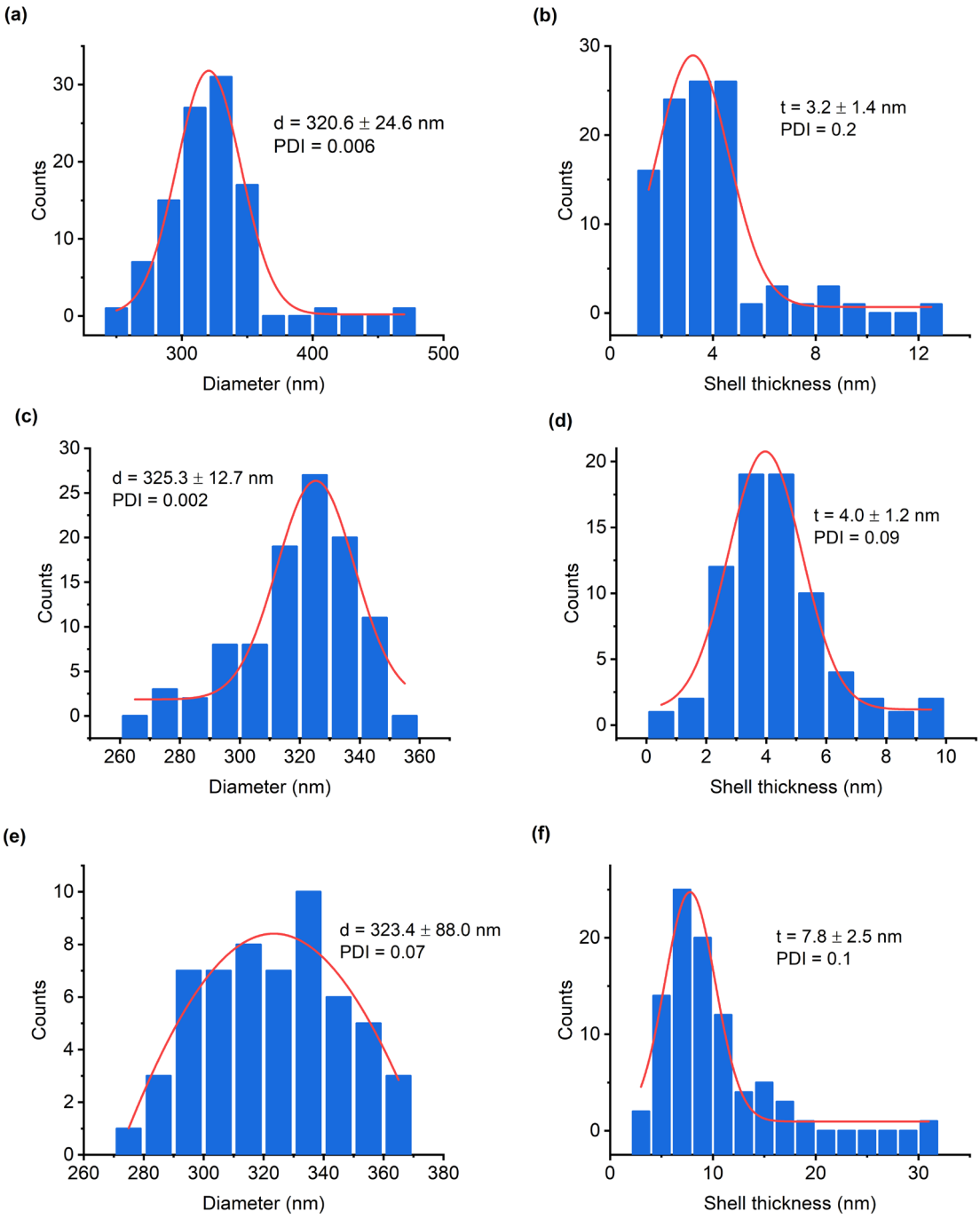

Fig. S12. Particles size and shell thickness distribution and Gaussian fit for **M1bIm** (a, b), **N1bIm** (c, d), **M2bIm** (e, f), **N2bIm** (g, h), **M3bIm** (i, j) and **N3bIm** (k, l) core-shell polymer@SiO_2 particles; **M1bIM**, **N1bIm**, **M2bIm**, **N2bIm,** **M3bIm** and **N3bIm** size and shell thickness distribution – blue bars, Gaussian fit of distribution – red line. (Continued on next page.)

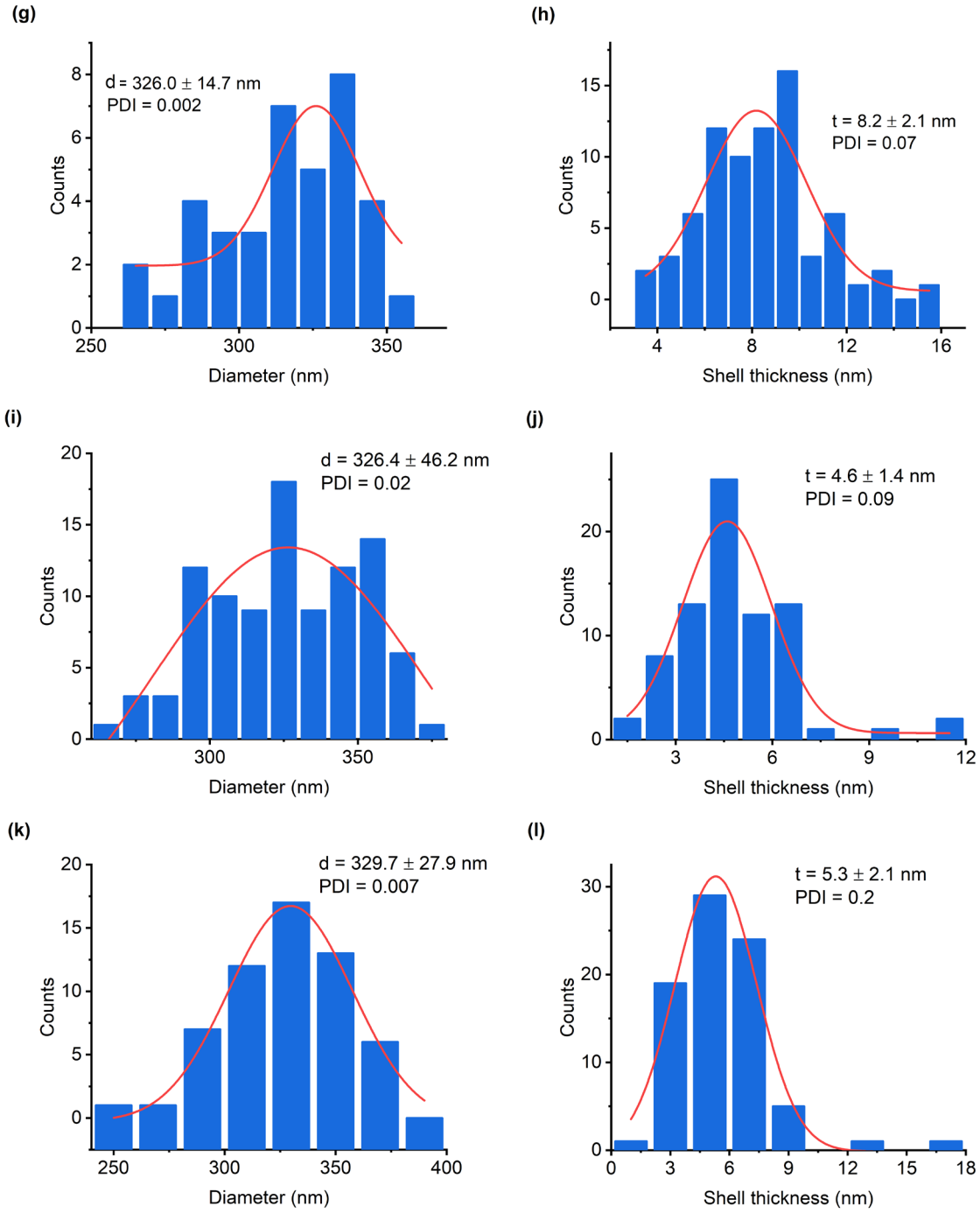

Fig. S12 (continued). (Caption shown on previous page.)

S6. Characterisation of functionalisation of core SiO_2 particles by DLS and TGA

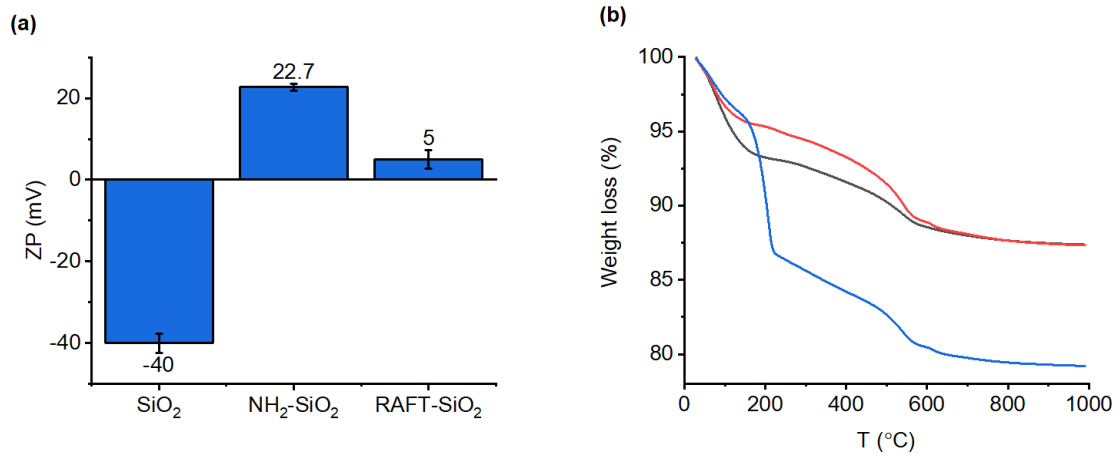

Fig. S13. Zeta potential change (a) and TGA curves (b) for the core and functionalised SiO_2 particles; core SiO_2 particles – black line, NH_2-SiO_2 particles – red line and RAFT-SiO_2 particles – blue line. Error bars are standard deviations for three replicates.

Fig. S13a shows that after the introduction of NH_2 groups, the net charge increases from –40.0 mV to +22.7 mV due to their partial protonation. After condensation with the RAFT agent, the effective charge decreases again through transformation of primary amines to amides.

Fig. S13b collects the corresponding TGA profiles. The weight loss up to 200 °C is due to adsorbed water and organic solvents on the surface of the particles, which are not completely removed even after the prolonged drying in a vacuum oven.[18] The total weight loss is 13% and 21% for the NH_2- and RAFT-SiO_2 particles, respectively. The thermogram for NH_2-SiO_2 particles includes three degradation stages. The first one is around 250 °C as physically adsorbed APTES is evaporating from the particles, the second stage at about 650 °C is due to the thermal decomposition of the organic part of the particles, and above 650 °C the dihydroxylation of the SiO_2 core is taking place. For the RAFT-SiO_2 particles, the decomposition of the RAFT agent can be seen up to 200 °C due to the thermal cleavage of the weak sulphur-carbon bond.[19] Since in this temperature region the adsorbed water and organic solvent molecules are leading to a weight loss as well, quantification of attached RAFT molecules is not possible with TGA in the presented case, even if it is commonly used for that.[20]

As an alternative method, elemental analysis can be employed to estimate the number of functional groups as it allows to calculate the real amount of the elements present. By evaluating the sulphur (0.12%) content of the RAFT-SiO_2 particles the number of functional groups on the surface can be estimated via Equation S2, using the BET specific surface area of the SiO_2 core particles (16.4 $m^2\ g^{-1}$). The number of RAFT groups was calculated to be 0.67 nm^{-2}. Here, *%w* is the weight percentage of sulphur obtained from elemental analysis (0.12%), *MW* – molecular weight of sulphur (32 mol g^{-1}), *n* – number of sulphur atoms in the molecule (2), N_A - Avogadro's number and S_{BET} - specific surface area of SiO_2 core particles obtained from nitrogen adsorption (16.4 $m^2\ g^{-1}$).

Equation S2. Functional groups estimation using elemental analysis.

$$C_{functional\ groups} = \frac{\%w}{100\% \cdot MW \cdot n} \cdot \frac{N_A}{S_{BET}} \cdot 10^{-18} (nm^{-2})$$

S7. Prepolymerisation studies and post-synthetic treatment of MIP and NIP core-shell polymer@SiO_2particles

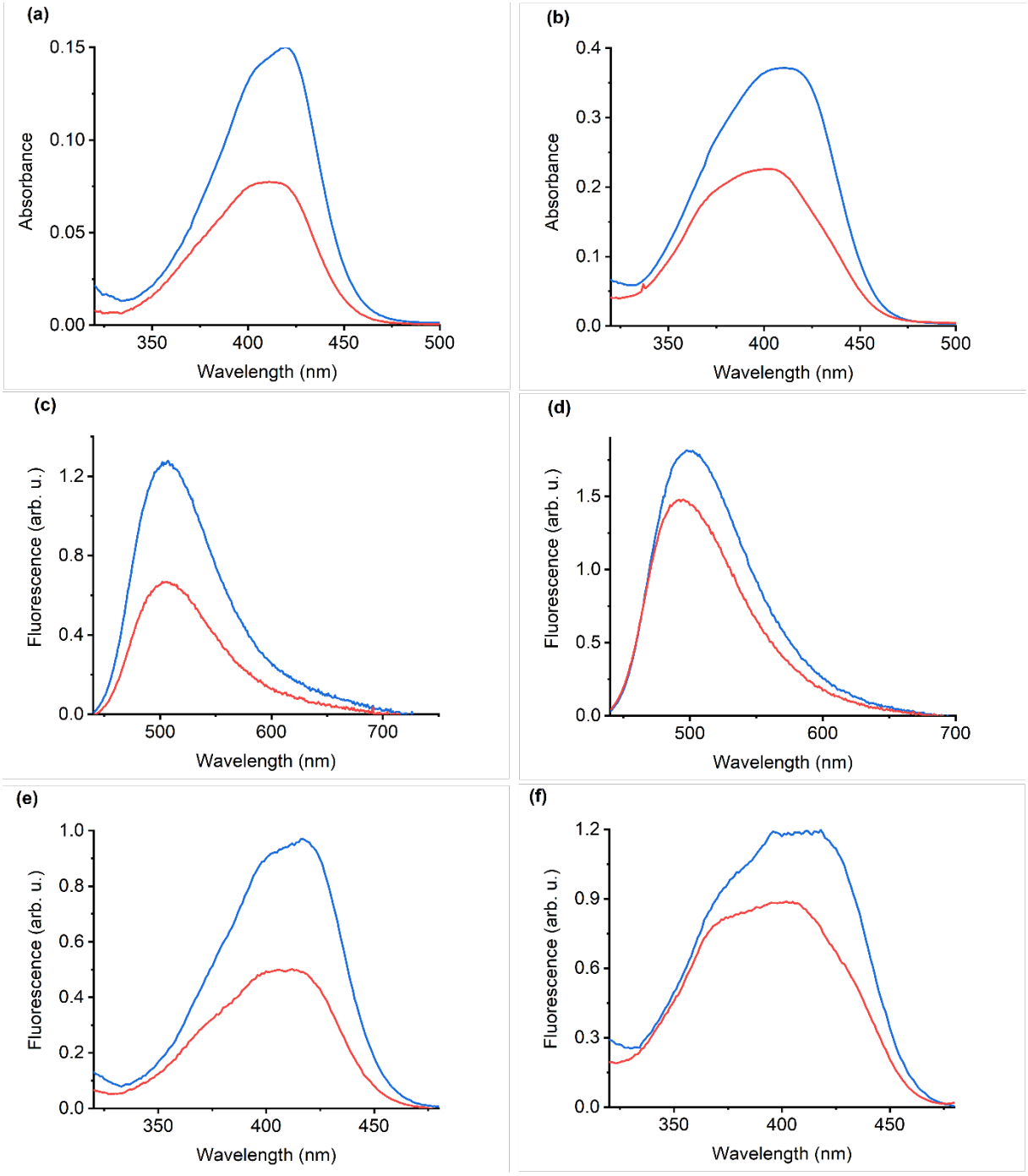

Fig. S14. Absorption, fluorescence emission (λ_{exc} = 385 nm) and excitation (λ_{em} = 490 nm) spectra of pre-polymerisation mixture for **M1bIm** and **N1bIm** (a, c, e) and for **M2bIm** and **N2bIm** (b, d, f) core-shell polymer@SiO_2 particles; **M1bIm** and **M2bIm** – blue line, **N1bIm** and **N2bIm** – red line.

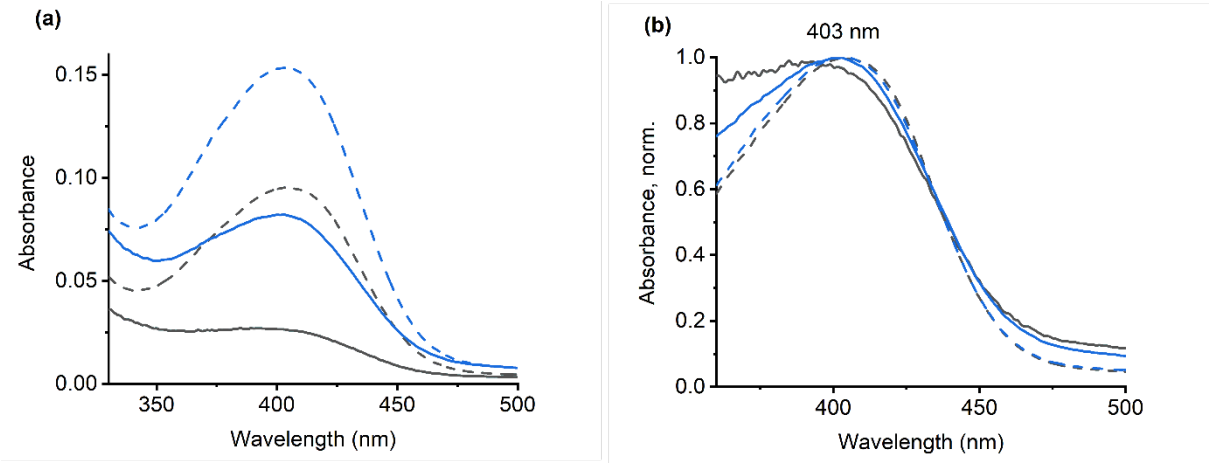

Fig. S15. Absorption (a) and normalised absorption (b) of **M1bIm**, **N1bIm**, **M2bIm** and **N2bIm** core-shell polymer@SiO_2 particles (0.5 mg ml^{-1}) in chloroform after washing; **M1bIm –** black line, **N1bIm** – dashed black line, **M2bIm –** blue line and **N2bIm** – dashed blue line.

S8. Calculation of the molar absorption coefficient of fCL[21]

The molar absorption coefficient of fluorescent probe cross-linker **fCL** in chloroform was calculated using the Beer-Lambert law (Equation S3), where *A* is the absorption of fluorophore in chloroform, *c* the dye concentration and *l* the optical path length of the cuvette. The absorption spectra were recorded for three stock solutions of fluorophore (7.39 µM) in chloroform with two replicates in the quartz cuvette with 1 cm optical path length (Fig. S16). The coefficient at λ_{max} = 401 nm was calculated as 13638 ± 573 $M^{-1}\,cm^{-1}$.

Equation S3. Beer-Lambert law.

$$\varepsilon = \frac{A}{c \cdot l}\ (M^{-1} \cdot cm^{-1})$$

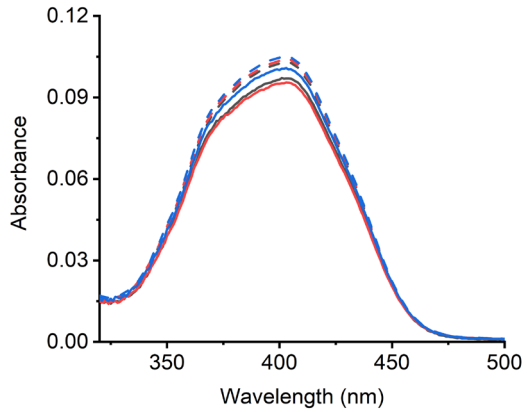

Fig. S16. Absorption spectra of three stock solutions in two replicates of **fCL** (7.39 µM) in chloroform; sample 1.1 – black line, 1.2 – dashed black line, 2.1 – red line, 2.2 – dashed red line, 3.1 – blue line, 3.2 – dashed blue line.

S9. Calculation of the amount of fCL in the polymer shell

To estimate the amount of fluorescent probe **fCL** in the polymer shell the absorption spectra of **M1bIm**, **N1bIm**, **M2bIm** and **N2bIm** core-shell polymer@SiO_2 particles were corrected using the 9-point method.[20] Absorption at 320, 325, 330, 340, 470, 475, 480, 490, 500 nm were chosen for the baseline correction for each spectra with an additional absorption at λ = 401 nm as a reference. 9 points were fitted using a non-linear exponential function and the fit was used for the baseline subtraction of the particles' absorption (Fig. S17).

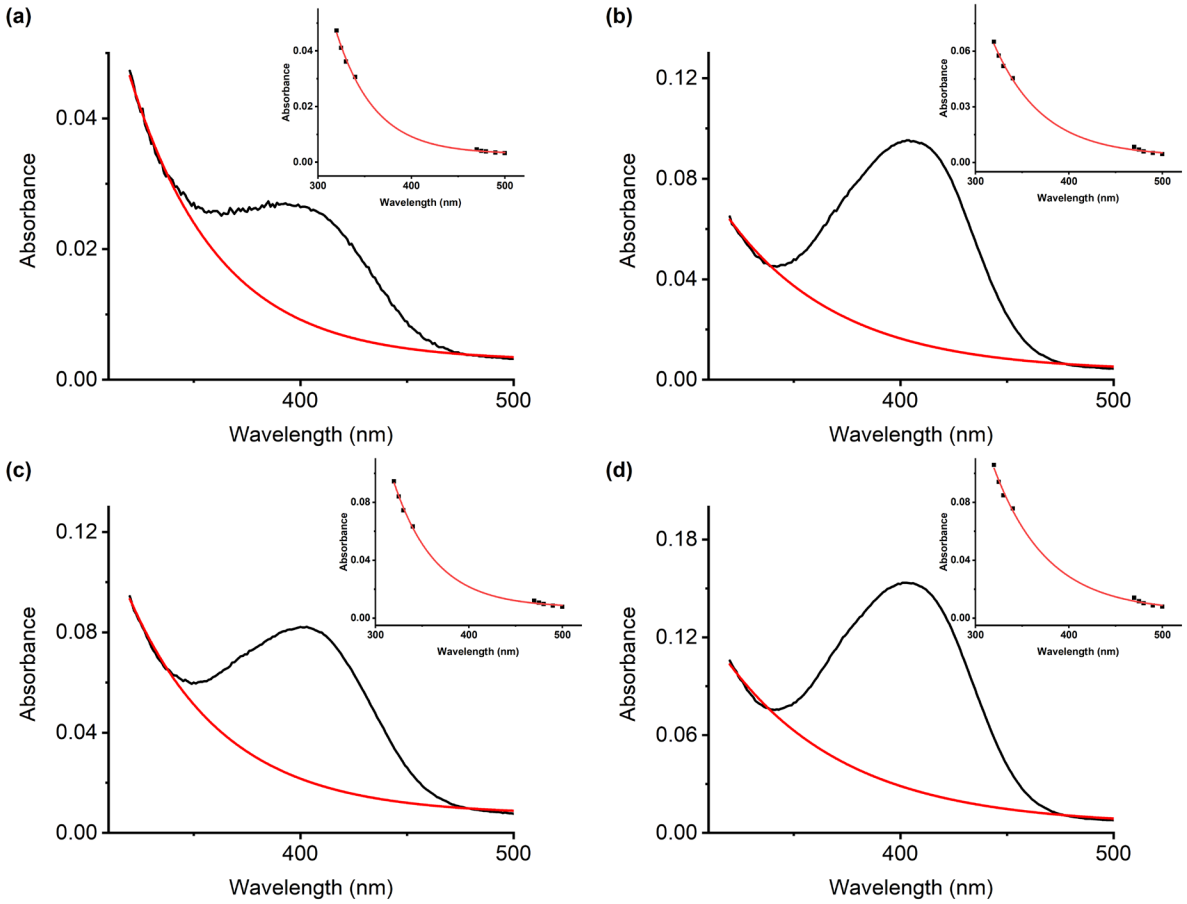

Fig. S17. Absorption spectra of **M1bIm** (a), **N1bIm** (b), **M2bIm** (c) and **N2bIm** (d) core-shell polymer@SiO_2 particles (0.5 mg ml^{-1}) in chloroform; **M1bIm**, **N1bIm**, **M2bIm** and **N2bIm** – black line, exponential fit of the baseline – red line, 9-point exponential fit – in the insert.

Concentration of **fCL** in the particles was calculated using Equation S4, with A_{401} – particles absorption at λ = 401 nm from the corrected absorption spectra (Fig. S18), ε_{401} – molar absorption coefficient of probe **fCL** at λ = 401 nm (13638 $M^{-1}\,cm^{-1}$), l – optical path length of the cuvette (1 cm) and $c_{particles}$ – the particles concentration in the cuvette (0.5 mg ml^{-1}).

Equation S4. Calculation of concentration of **fCL** in MIP and NIP core-shell polymer@SiO_2 particles.

$$C_{fCL} = \frac{A_{401}}{\varepsilon_{401} \cdot l \cdot c_{particles}} \cdot 10^{-3} (\mu mol/mg_{particles})$$

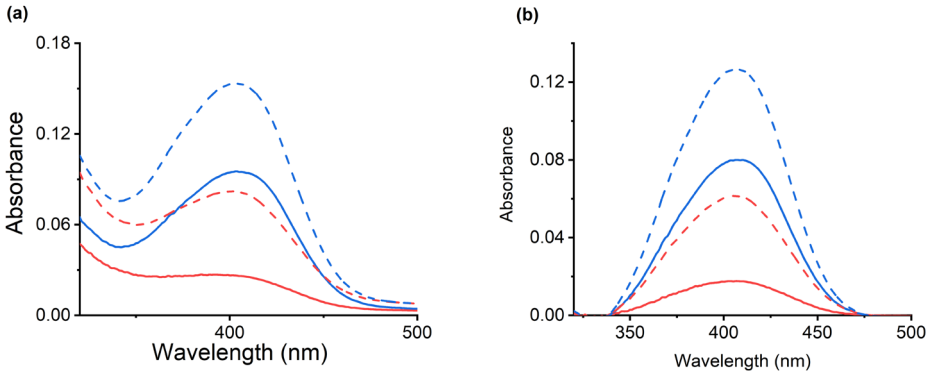

Fig. S18. Uncorrected (a) and corrected (b) absorption spectra of **M1bIm**, **N1bIm**, **M2bIm** and **N2bIm** core-shell polymer@SiO_2 particles (0.5 mg ml^{-1}) in chloroform; **M1bIm –** solid red line, **N1bIm** – solid blue line, **M2bIm –** dashed red line and **N2bIm** – dashed blue line.

To calculate the fluorophore concentration in the polymer, the shell weight needs to be calculated first. Using the shell thickness from the TEM images, the polymer weight can be estimated using Equation S5, with d_{core} – diameter of the SiO_2 core particles, $D_{particle}$ – diameter of the core-shell polymer@SiO_2 particles, t_{shell} – polymer shell thickness, V_{core} – SiO_2 core volume, $V_{particle}$ – core-shell polymer@SiO_2 volume, V_{shell} – polymer shell volume, S_{core} – surface area of SiO_2 core, S_{BET} – BET specific surface area of SiO_2 core (16.4 $m^2\,g^{-1}$), m_{core} – SiO_2 core weight and ρ_{shell} – density of polymer shell (assuming 1 g cm^{-3}). The results are summarised in Table S5.

Equation S5. Calculation of estimated shell weight percentage.

$$d_{core} = (D_{particle} - 2 \cdot t_{shell}) \cdot 10^{-9} (m^3)$$

$$V_{core} = \frac{4}{3}\pi \left(\frac{d_{core}}{2} \cdot 10^{-9}\right)^3 (m^3)$$

$$V_{particle} = \frac{4}{3}\pi \left(\frac{D_{particle}}{2} \cdot 10^{-9}\right)^3 (m^3)$$

$$V_{shell} = V_{particle} - V_{core}\ (m^3)$$

$$S_{core} = 4\pi \left(\frac{d_{core}}{2} \cdot 10^{-9}\right)^2 (m^2)$$

$$m_{core} = \frac{S_{core}}{S_{BET}}\ (g)$$

$$shell\ w\% = \frac{V_{shell} \cdot \rho_{shell}}{m_{core}} \cdot 10^6 \cdot 100\%\ (\%)$$

Table S5. Fluorescent probe **fCL** concentration in the shell of MIP and NIP core-shell polymer@SiO_2 particles.

Sample	c, µM	c, µmol mg^{-1}particles	Shell, wt%	c, µmol mg^{-1} polymer shell
M1bIm	1.28	0.0026	5.36	0.048
N1bIm	5.77	0.015	6.73	0.17
M2bIm	4.45	0.0089	13.45	0.066
N2bIm	9.18	0.018	14.17	0.13

S10. Spectroscopic properties and response behavior of MIP and NIP core-shell polymer@SiO_2 particles

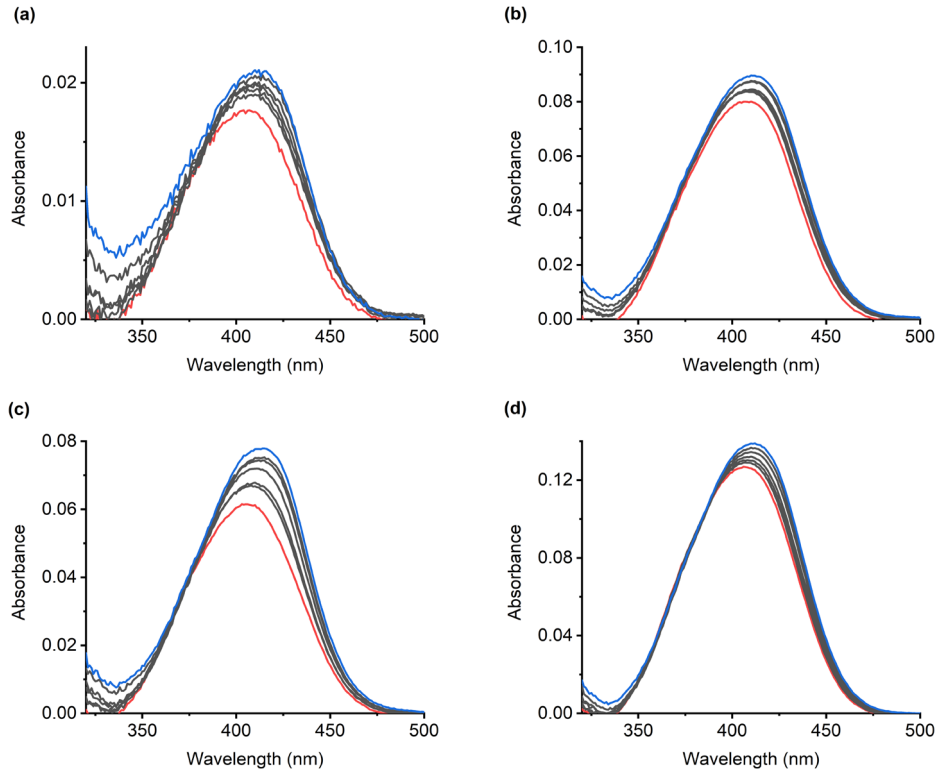

Fig. S19. Corrected absorption spectra of **M1bIm** (a), **N1bIm** (b), **M2bIm** (c) and **N2bIm** (d) core-shell polymer@SiO_2 particles (0.5 mg ml^{-1}) in chloroform upon addition of an increasing amount of Fmoc-Y-pY-G-OMe-TBA (0–69.8 µM) in chloroform; **M1bIm**, **N1bIm**, **M2bIm** and **N2bIm** – red line, **M1bIm**, **N1bIm**, **M2bIm** and **N2bIm** and 69.8 µM of Fmoc-Y-pY-G-OMe-TBA – blue line.

To calculate the strength of interaction between MIP core-shell polymer@SiO_2 particles and Fmoc-Y-pY-G-OMe-TBA increasing concentrations of analyte were added to 0.5 mg ml^{-1} suspensions of **M1bIm** and **M2bIm** in chloroform and the absorption data (Fig. S19) were fitted using a 1:1 (host:guest) non-linear binding model with BindFit software. The binding constant were calculated to 269578 ± 16826 M^{-1} and 239437 ± 9603 M^{-1}, respectively.

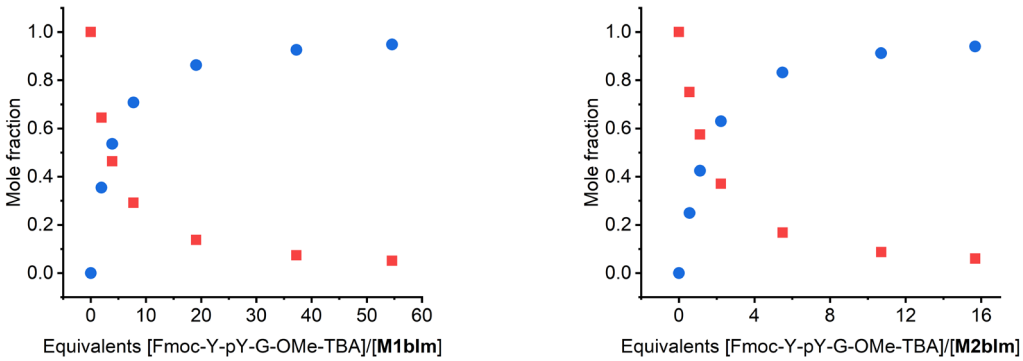

Fig. S20. Relative species concentration during the titration of 0.5 mg ml^{-1} suspension of **M1bIm** (left) and **M2bIm** (right) core-shell polymer@SiO_2 particles in chloroform (equiavlent to **fCL** concentrations of is 1.3 and 4.4 µM) with an increasing amount of Fmoc-Y-pY-G-OMe-TBA in chloroform as derived from BindFit fitting; **M1bIm**/**M2bIm** – red ■, complex – blue ●.

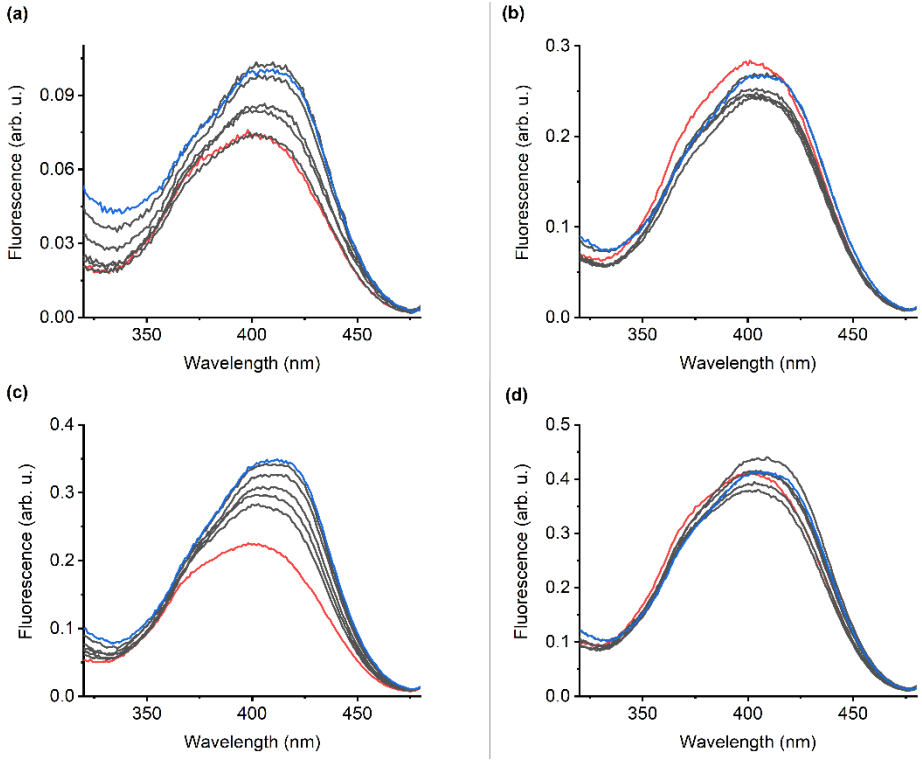

Fig. S21. Fluorescence excitation (λ_{em} = 490) spectra of **M1Im** (a), **N1bIm** (b), **M2bIm** (c) and **N2bIm** (d) core-shell polymer@SiO_2 particles (0.5 mg ml^{-1}) in chloroform upon addition of an increasing amount of Fmoc-Y-pY-G-OMe-TBA (0–69.8 µM) in chloroform; **M1Im**, **N1bIm**, **M2bIm** and **N2bIm –** red line, **M1Im**, **N1bIm**, **M2bIm** and **N2bIm** and 69.8 µM of Fmoc-Y-pY-G-OMe-TBA **–** blue line. These spectra complement the absorption spectra in Fig. S20 and the fluorescence spectra in Fig. 5.

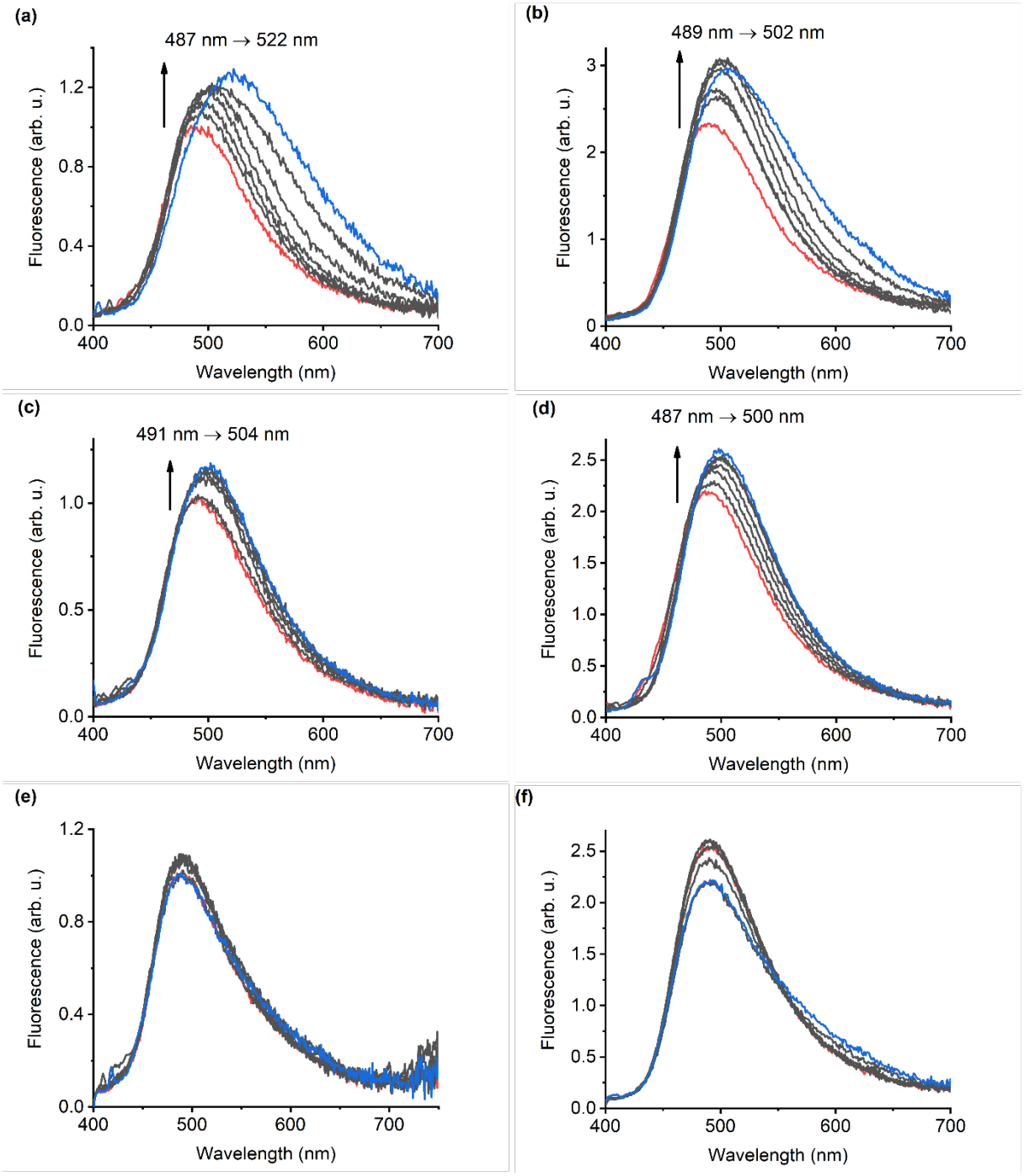

Fig. S22. Fluorescence emission (λ_{exc} = 385 nm) spectra of **M1bIm** and **M2bIm** core-shell polymer@SiO_2 particles (0.5 mg ml^{-1}) in chloroform upon addition of an increasing amount of HPPA-TBA (a, b), HPPA-THA (c, d) and Fmoc-Y-Y-G-OMe (e, f) (0–69.8 µM) in chloroform; **M1bIm** and **M2bIm –** red line, **M1bIm** and **M2bIm** and 69.8 µM of HPPA-TBA, HPPA-THA and Fmoc-Y-Y-G-OMe **–** blue line.

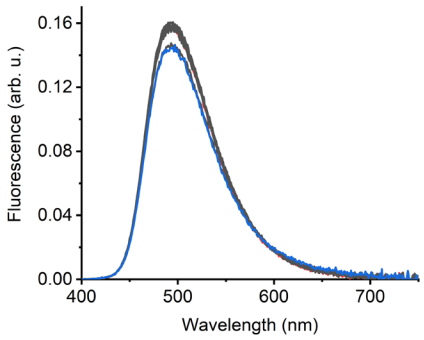

Fig. S23. Fluorescence emission (λ_{exc} = 385 nm) spectra of **fCL** (1.67 µM) in chloroform upon addition of an increasing amount of Fmoc-Y-Y-G-OMe (0–44.8 eq.) in chloroform; **fCL** – red line and **fCL** and 44.8 eq. of Fmoc-Y-Y-G-OMe – blue line.

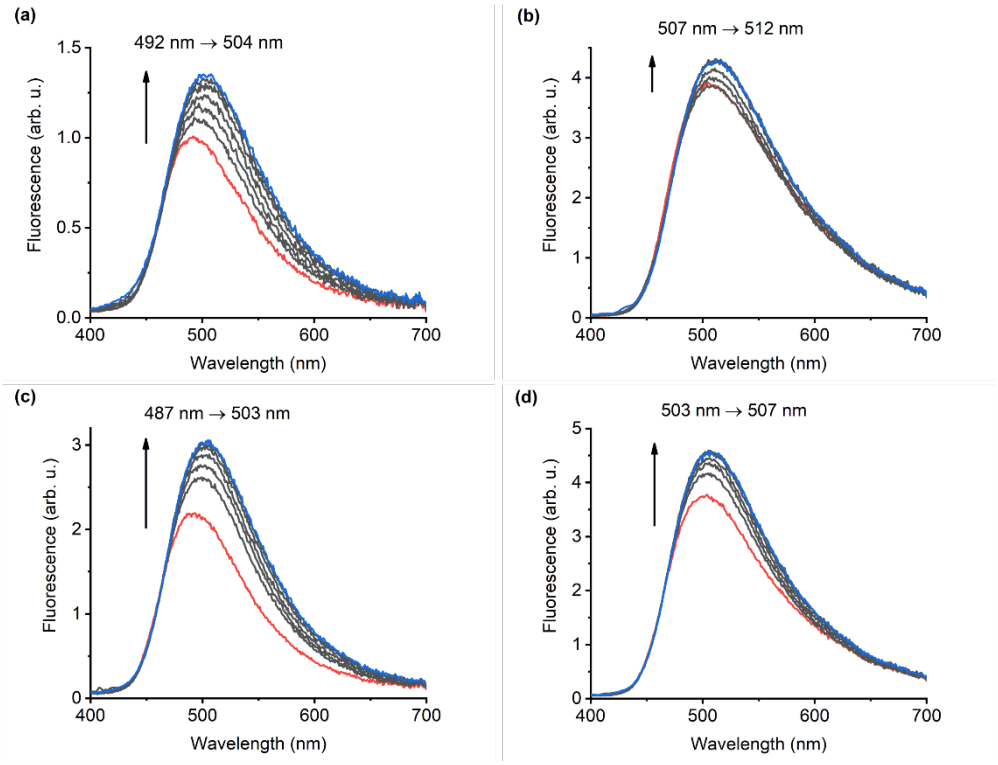

Fig. S24. Fluorescence emission (λ_{exc} = 385 nm) spectra of **M1bIm** (a), **N1bIm** (b), **M2bIm** (c) and **N2bIm** (d) core-shell polymer@SiO_2 particles (0.5 mg ml^{-1}) in chloroform upon addition of an increasing amount of Fmoc-pY-OEt-TBA (0–69.8 µM) in chloroform; **M1bIm**, **N1bIm**, **M2bIm** and **N2bIm –** red line, **M1bIm**, **N1bIm**, **M2bIm** and **N2bIm** and 69.8 µM of Fmoc-pY-OEt-TBA **–** blue line.

S11. Spectroscopic properties and response behavior of additional "no" and "D" MIP and NIP core-shell polymer@SiO_2 particle batches

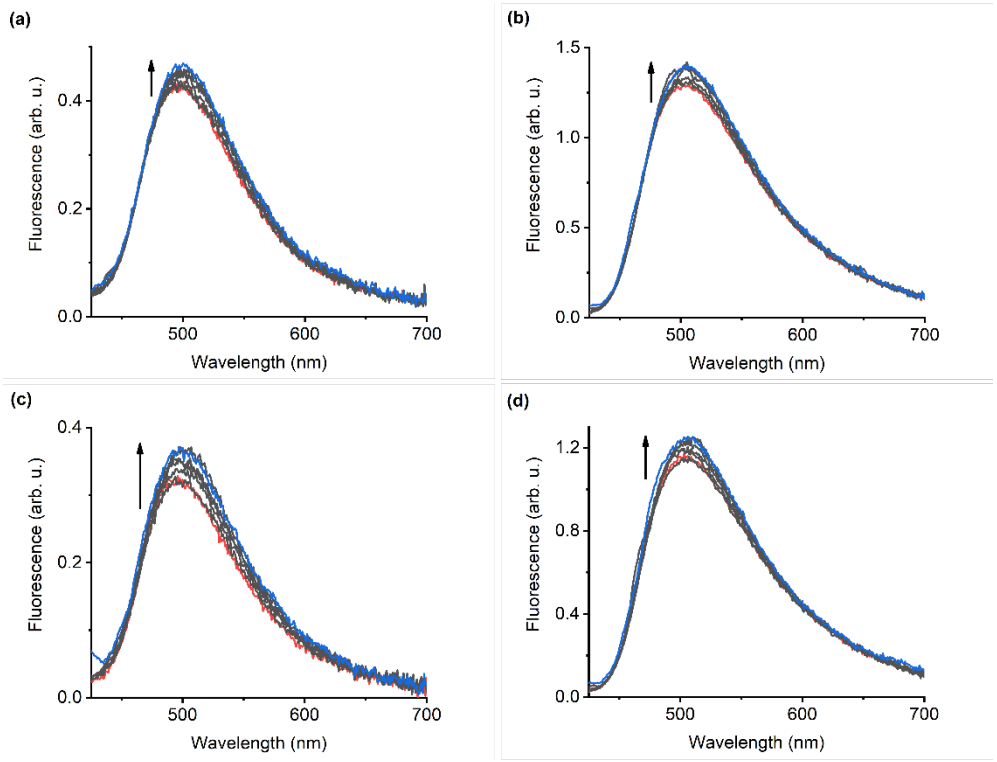

Fig. S25. Fluorescence emission (λ_{exc} = 385 nm) spectra of **M1no** (a), **N1no** (b), **M1D** (c) and **N1D** (d) core-shell polymer@SiO_2 particles (0.5 mg ml^{-1}) in chloroform upon addition of an increasing amount of Fmoc-Y-pY-G-OMe-TBA (0–69.8 µM) in chloroform; **M1no**, **N1no**, **M1D** and **N1D** – red line, **M1no**, **N1no**, **M1D** and **N1D** and 69.8 µM of Fmoc-Y-pY-G-OMe-TBA – blue line.

S12. Binding mechanism of MIP particles in chloroform

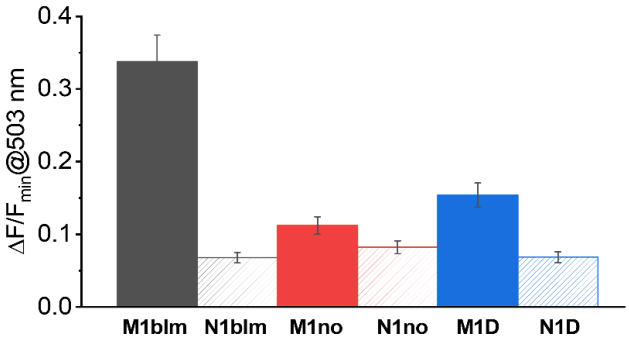

Fig. S26. Overview of fluorescence emission intensity changes at λ = 503 nm for **M1bIm**, **N1bIm**, **M1no**, **N1no**, **M1D** and **N1D** core-shell polymer@SiO_2 particles (0.5 mg ml^{-1}) in chloroform upon addition of 69.8 µM of Fmoc-Y-pY-G-OMe-TBA in chloroform; **M1bIm** and **N1bIm** - black filled and shaded bar, respectively, **M1no** and **N1no** - red filled and shaded bar, respectively, and **M1D** and **N1D** - blue filled and shaded bar, respectively. Measurement uncertainties as indicated for selected bars and related molecules. $\Delta F/F_{min} = (F_x - F_{min})/F_{min}$.

For this system, the recognition of analytes by MIPs primarily relies on hydrogen bonding to the urea moiety of the fluorescent cross-linker **fCL**. In contrast, the binding between **bIm-PF$_6$** and the phosphate anions is less probable. To determine the strength of interaction between **bIm-PF$_6$** and the model anlayte HPPA-TBA, a solution of bis-imidazolium monomer in DMSO-d_6 (5 mM) was used, and increasing concentrations of analyte (0–10 eq.) in DMSO-d_6 were added. The chemically induced shifts (CIS) for multiple protons were analysed by them with a 1:1 (host:guest) non-linear binding model using BindFit software (Fig. S27). The binding constant was calculated as K_a = 109 ± 4 M^{-1} (Fig. S28), which is slightly lower than the K_a value obtained for **bIm-Br** in a previous study.[4] This suggests that during the titration experiment, binding of the analyte to the urea group is more likely than interaction with the bis-imidazolium moiety. However, cross-selectivity experiments revealed that additional π-π interactions contribute to the rebinding of analytes to the polymer shell, indicating that the bis-imidazolium moiety and the urea groups are in proximity within the polymer network. Furthermore, the MIPs prepared without **bIm-PF$_6$** did not show a high affinity towards the tripeptide analyte, indicating that template interaction with both **bIm-PF$_6$** and **fCL** during the polymerisation process plays a role.

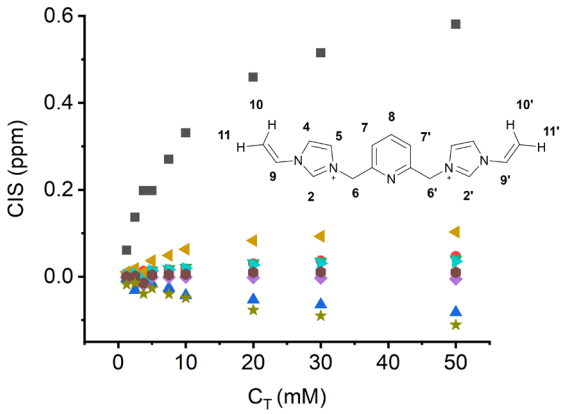

Fig. S27. CIS for multiple protons during the titration of 5 mM of **bIm-PF$_6$** in DMSO-d_6 with an increasing amount of HPPA-TBA (0–10 eq.) in DMSO-d_6; H2/2' – black ■, H4/4' – red ●, H5/5' – green ▼, H6/6' – dark brown ⬢, H7/7' – purple ◆, H8 – blue ▲, H9/9' – light brown ◀, H10/10' – cyan ▶ and H11/11' – olive ★. CIS – chemically induced shift. C_T – concentration of template.

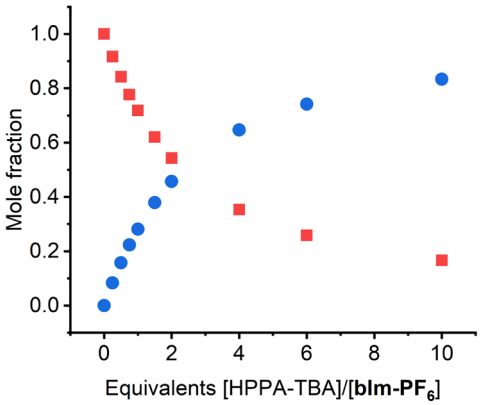

Fig. S28. Relative species concentration during the titration of 5 mM of **bIm-PF$_6$** in DMSO-d$_6$ with an increasing amount of HPPA-TBA (0–10 eq.) in DMSO-d$_6$; **bIm-PF$_6$** – red ■ and complex – blue ●.

To understand the cooperative binding mechanism, Hard-Soft Acid-Base (HSAB) theory, also known as Pearson's theory, can be employed.[22] During complex formation between the template and the functional urea cross-linker, the attractive force exerted on an analyte is strong enough to dissociate the molecule, which exists as an ion pair.[23] The phosphate anion forms highly directional hydrogen bonds with the urea, as depicted in Scheme S4. At the same time, the loosely bound TBA$^+$ cation can interact with other anions present in the pre-polymerisation mixture. TBA$^+$ acts as a soft acid and readily forms an ion pair with soft bases in the system, such as the hexafluorophosphate anion.[24] Simultaneously, the ion binding strength in **bIm-PF$_6$** between the PF_6^- (soft base) and the bis-imidazolium fragment (soft acid)[24] is sufficient to ensure that the entire ion pair is situated in close proximity to the ternary system of the template anion, the counter-cation, and urea cross-linker (Scheme S4). Additional π-π stacking and hydrogen bond interactions between the template and bis-imidazolium further reinforce the arrangement of urea and imidazolium cross-linkers in close proximity. However, interactions between imidazolium cations and phosphate anions are less likely due to a hardness mismatch according to HSAB theory, with the phosphate anion being a hard base and imidazolium cations being a soft acid. Alternatively, the presence of PF_6^- may promote the dissociation of the ion pair of the template first, facilitating the complex formation between the phosphate anion and the urea cleft of **fCL** (Scheme S4).

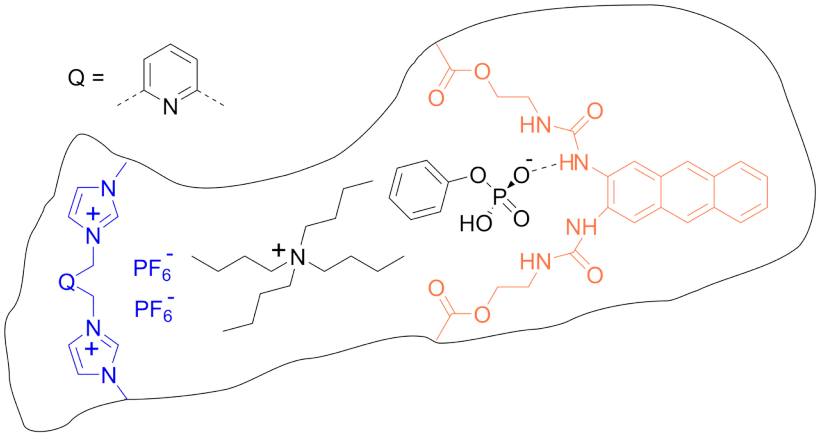

Scheme S4. Proposed model of imprinted cavity in **M1bIm** and **M2bIm** core-shell polymer@SiO$_2$ particles .

S13. Peptides used in capture studies

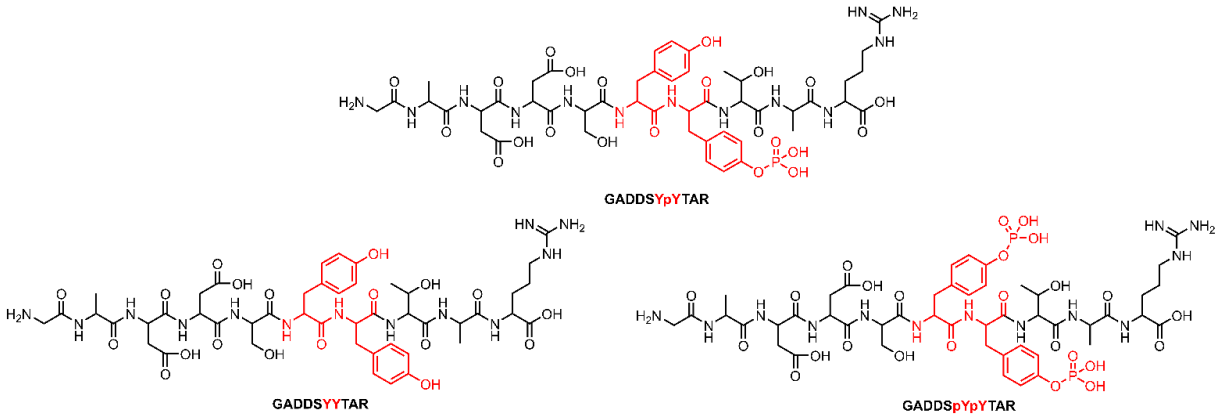

Scheme S5. Structures of decapeptides used for the capture experiments in aqueous media.

S14. Calculation of the pK_a values of fCL[25]

The pK_a values of the fluorescent probe cross-linker **fCL** were calculated from the absorption spectra at different pH. Solutions of **fCL** (16 µM) in spectroscopic ethanol/Milli-Q water 1:1 v/v solution were prepared by adding 40 µl of a 1 mM stock solution of the **fCL** to 10×10 mm quartz cells containing 2.5 mL of a solvent mixture. Aliquots of 0.01–1 M potassium hydroxide or 0.01–1 M perchloric acid in the solvent mixture were added to the solutions, while the pH was constantly monitored with a digital pH meter equipped with a glass electrode and calibrated with standard aqueous solutions of pH 4.01, 7.01 and 9.00. Absorption spectra were taken after the addition of each aliquot. For data analysis, pH values in the solvent mixture were activity-corrected (Fig. S29).[25] The final pK_a values were determined to 0.99 ± 0.01 for the conjugated acid of the fluorescent probe cross-linker **fCL**H^+ upon protonation of a nitrogen of the phenazine system[26] and 11.92 ± 0.01 for the anionic form of **fCL**$^-$ upon the deprotonation of one of the urea groups (Scheme S6).

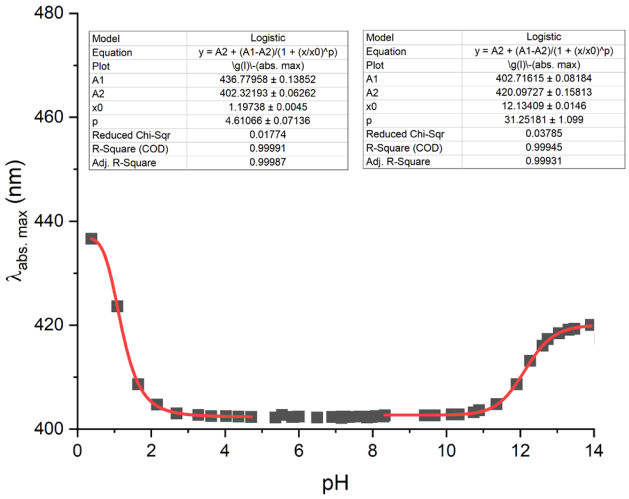

Fig. S29. pH curve titration for fluorescent probe **fCL**; absorption maximum of fluorescent probe **fCL** at indicated pH – black ■, logistic fit – red line.

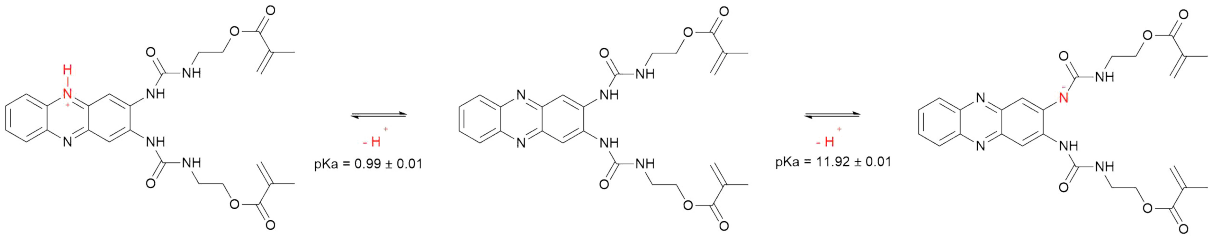

Scheme S6. Protonation/deprotonation equilibria of fluorescent probe cross-linker **fCL** in the commonly relevant pH window 0–14.

S15. Determination of LOB, LOD and LOQ of M1bIm core-shell polymer@SiO_2 particles

To determine limit of blank (*LOB*), limit of detection (*LOD*) and limit of quantitation (*LOQ*) the fluorescence emission (λ_{exc} = 385 nm) response at λ = 503 nm of **M1bIm** core-shell polymer@SiO_2 particles (0.5 mg ml^{-1}) in chloroform upon addition of an increasing amount of Fmoc-Y-pY-G-OMe-TBA (0–69.8 µM) in chloroform (Fig. 6a) was plotted and fitted using a logistic function (Fig. S30).

From the fitting equation, the concentration corresponding to the fluorescence emission of three blank measurements of 0.5 mg ml^{-1} **M1bIm** in chloroform was used to determine the *LOB* (Equation S6), where $\bar{x}_{blank}$ is a mean concentration corresponding to the blank measurements and SD_{blank} is a standard deviation for the mean concentration corresponding to the blank measurements.

Three repeat measurements of the lowest concentration used (2.49 µM) were used to determine the *LOD* (Equation S6). *LOQ* was calculated using blank measurements (Equation S6).[27]

The values were calculated as: *LOB* = 4.24 µM, *LOD* = 11.16 µM and *LOQ* = 13.02 µM.

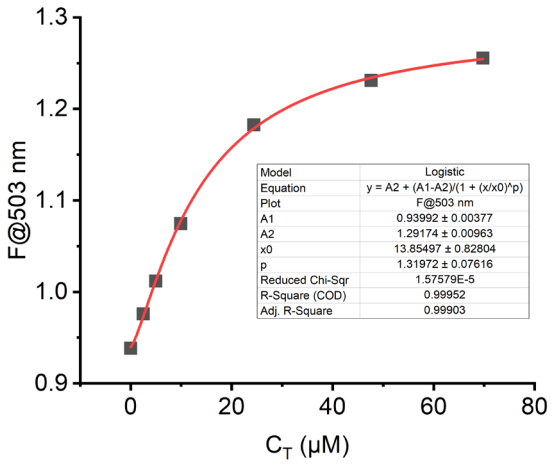

Fig. S30. Logistic curve fitting of emission at λ = 503 nm (λ_{exc} = 385 nm) of **M1bIm** core-shell polymer@SiO_2 particles (0.5 mg ml^{-1}) in chloroform upon addition of an increasing amount of Fmoc-Y-pY-G-OMe-TBA (0–69.8 µM) in chloroform; emission of **M1bIm** – black ■, logistic fit – red line. C_T – concentration of template.

Equation S6 *LOB*, *LOD* and *LOQ* calculation for **M1bIm** core-shell polymer@SiO_2 particles (0.5 mg ml^{-1}) in chloroform as blank and 2.49 µM of Fmoc-Y-pY-G-OMe-TBA in chloroform as the lowest concentration used.

$$LOB = \bar{x}_{blank} + 1.645 \cdot SD_{blank}\ (\mu M)$$

$$LOD = LOB + 1.645 \cdot SD_{lcs}\ (\mu M)$$

$$LOQ = 10 \cdot SD_{blank}\ (\mu M)$$

S16. Calculation of relative measurement uncertainties[21, 28]

Molar absorption coefficient of fCL

a) Relative uncertainties of preparation of 3 different stock solutions:
   - Weighing of ca. 0.15 mg fluorescent probe **fCL** for individual stock preparation (balance Satorius supermicro Type S4: ± 0.0001 mg); u_{rel}^{w} = 0.067%
   - Dissolving individual samples in ca. 1.5 ml of chloroform (Eppendorf Research plus pipette ± 0.03625 ml); u_{rel}^{d} = 2.42%

b) Relative uncertainties of preparation of measurement solution in a quartz cuvette:
   - Filling the cuvette with 2 ml of chloroform (Eppendorf Research plus pipette ± 0.03625 ml); u_{rel}^{f} = 1.81%
   - Addition of 80 µl of stock solutions to the cuvette (Eppendorf Research plus pipette ± 0.03625 ml); u_{rel}^{s} = 1.25%
   - Cell length contribution for a 10 mm optical path length quartz cell (± 0.01 mm); u_{rel}^{l} = 0.1%

c) For the absorption at λ_{401} ~ 0.1, the maximum possible error amounts to; $u_{rel}^{a} \leq 0.013\%$

d) Repeat accuracy of measurement (n = 6: ± 0.0017); u_{rel}^{i} = 1.73%

e) Experimental standard deviation for replicate measurements; $u_{rel}^{r} \leq 1.98\%$

f) Relative uncertainty of ε:

$$u_{rel}^{\varepsilon\,2} = u_{rel}^{w\,2} + u_{rel}^{d\,2} + u_{rel}^{f\,2} + u_{rel}^{s\,2} + u_{rel}^{l\,2} + u_{rel}^{a\,2} + u_{rel}^{i\,2} + u_{rel}^{r\,2}$$

$u_{rel}^{\varepsilon} \leq 4.20\%$

Particle titration experiment

a) Relative uncertainties of preparation of Fmoc-Y-pY-G-OMe-TBA and other templates:
   - Weighing of ca. 1 mg of neat template for template preparation (balance Mettler Toledo: ± 0.01 mg); u_{rel}^{w1} = 1%
   - Dissolving neat template in 1 ml of acetonitrile (Eppendorf Research plus pipette ± 0.008 ml); u_{rel}^{d1} = 0.8%
   - Weighing of ca. 10 mg of TBA-OH·30H_2O for stock preparation (balance Mettler Toledo: ± 0.01 mg); u_{rel}^{w2} = 0.1%
   - Dissolving TBA source in 1 ml of acetonitrile (Eppendorf Research plus pipette ± 0.008 ml); u_{rel}^{d2} = 0.8%
   - Addition of 0.1 ml of TBA-OH to the neat template (Eppendorf Research plus pipette ± 0.001 ml); u_{rel}^{s} = 1%

b) Relative uncertainties of preparation of template stock for the titration:
   - Dissolving TBA salt of template in 0.5 ml of chloroform (Eppendorf Research plus pipette ± 0.006 ml); u_{rel}^{t1} = 1.2%
   - Transferring 0.5 ml of template to the glass vial for measurement (Eppendorf Research plus pipette ± 0.006 ml); u_{rel}^{t2} = 1.2%
   - Diluting template to 1 mM stock solution with 1 ml of chloroform (Eppendorf Research plus pipette ± 0.008 ml); u_{rel}^{t3} = 0.8%

c) Relative uncertainties of preparation of particles stock solution:
   - Weighing of ca. 3 mg of particles (balance Mettler Toledo: ± 0.01 mg); u_{rel}^{w3} = 0.3%
   - Suspending particles in 3 ml of chloroform (Eppendorf Research plus pipette ± 0.03625 ml); u_{rel}^{d3} = 1.2%

d) Relative uncertainties of preparation of measurement solution in a quartz cuvette:
   - Addition of 1 ml of particles stock solutions to the cuvette (Eppendorf Research plus pipette ± 0.008 ml); u_{rel}^{p1} = 0.8%

- Diluting the suspension with 1 ml of chloroform (Eppendorf Research plus pipette ± 0.008 ml); u_{rel}^{p2} = 0.8%
- Cell length contribution for a 10 mm optical path length quartz cell (± 0.01 mm); u_{rel}^{l} = 0.1%

e) For the fluorescent intensity at λ_{503}, the maximum possible error amounts to; $u_{rel}^{f} \leq$ 0.28%:

f) Relative uncertainty for experiment repetition (n = 3, ± 0.16); $u_{rel}^{r} \leq$ 6.89%:

g) Error for the template addition (Eppendorf Research plus pipette $\leq$ ± 0.000115 ml); $u_{rel}^{a} \leq$ 2.3%

h) Relative uncertainty:

$$u_{rel}^{u}{}^{2} = u_{rel}^{w1}{}^{2} + u_{rel}^{d1}{}^{2} + u_{rel}^{w2}{}^{2} + u_{rel}^{d2}{}^{2} + u_{rel}^{s}{}^{2} + u_{rel}^{t1}{}^{2} + u_{rel}^{t2}{}^{2} + u_{rel}^{t3}{}^{2} + u_{rel}^{w3}{}^{2} + u_{rel}^{d3}{}^{2} + u_{rel}^{p1}{}^{2} + u_{rel}^{p2}{}^{2} + u_{rel}^{l}{}^{2} + u_{rel}^{f}{}^{2} + u_{rel}^{r}{}^{2} + u_{rel}^{a}{}^{2}$$

$u_{rel}^{u} \leq$ 7.90%

S17. NMR spectra

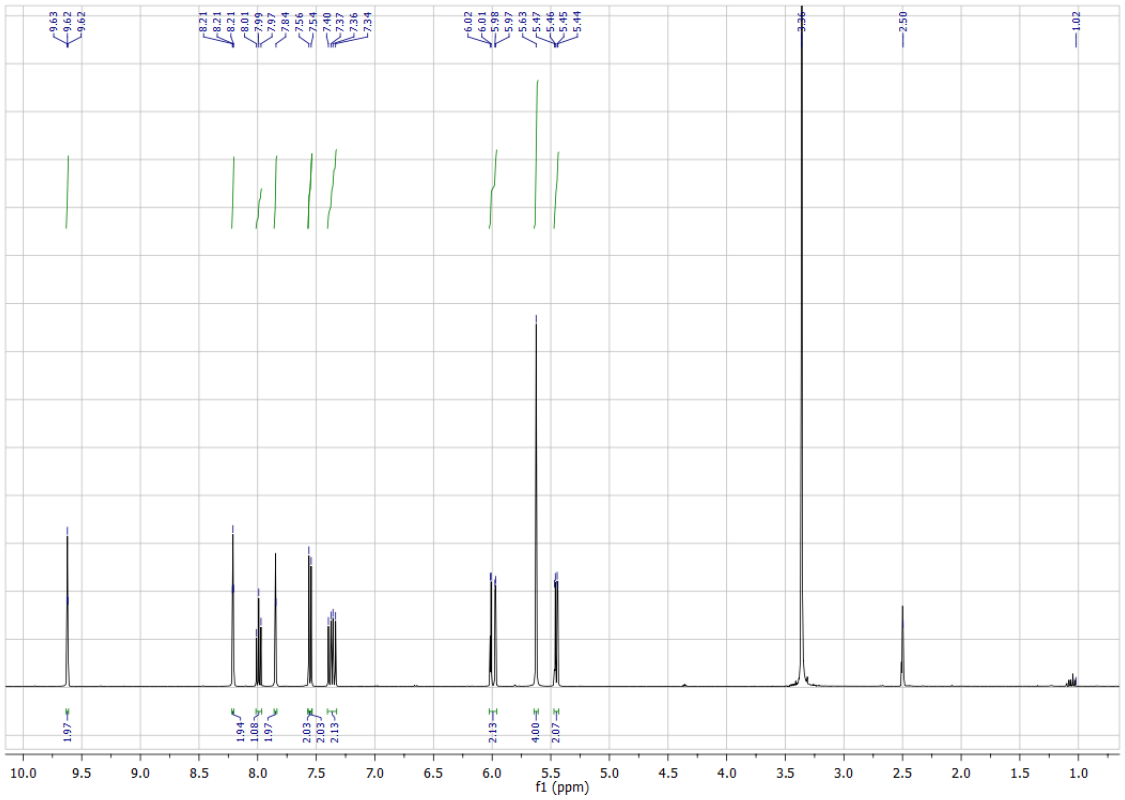

Fig. S31 ^{1}H NMR spectra of **bIm-Br** in DMSO-d_6 at 400 MHz (peak at 3.36 ppm is water and 1.10 ppm is H grease).[29]

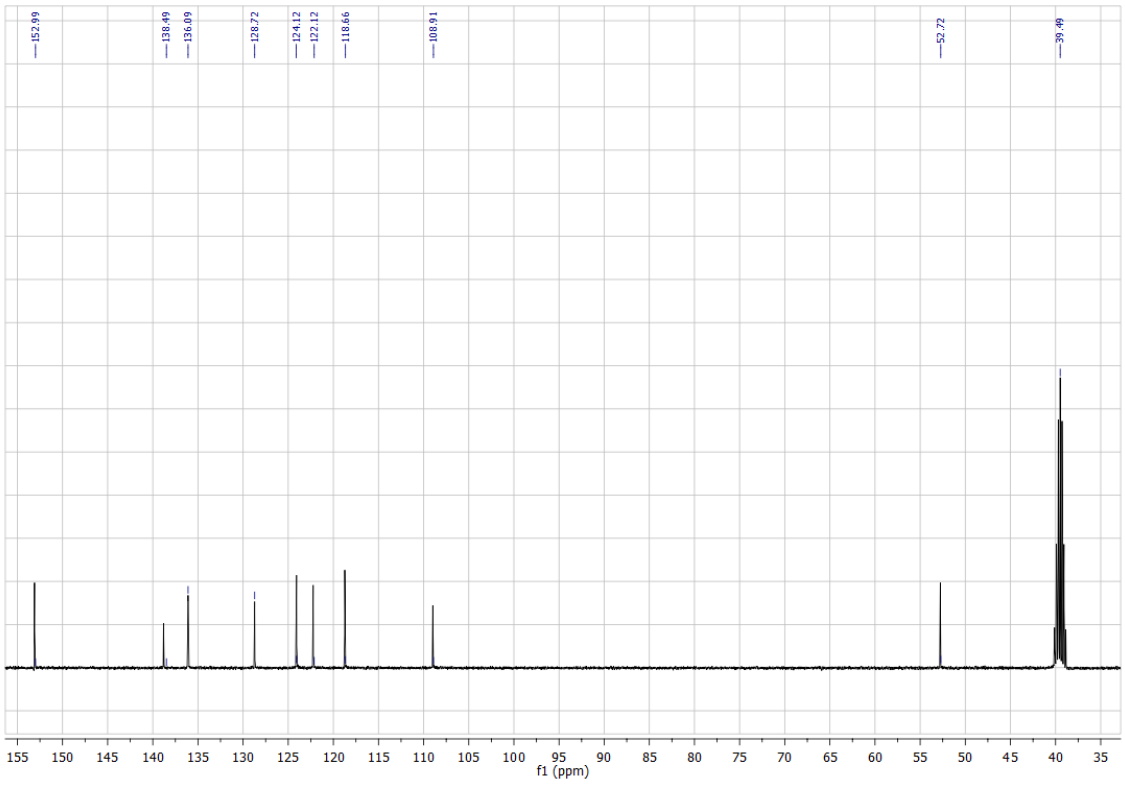

Fig. S32 ^{13}C NMR spectra of **bIm-Br** in DMSO-d_6 at 400 MHz.

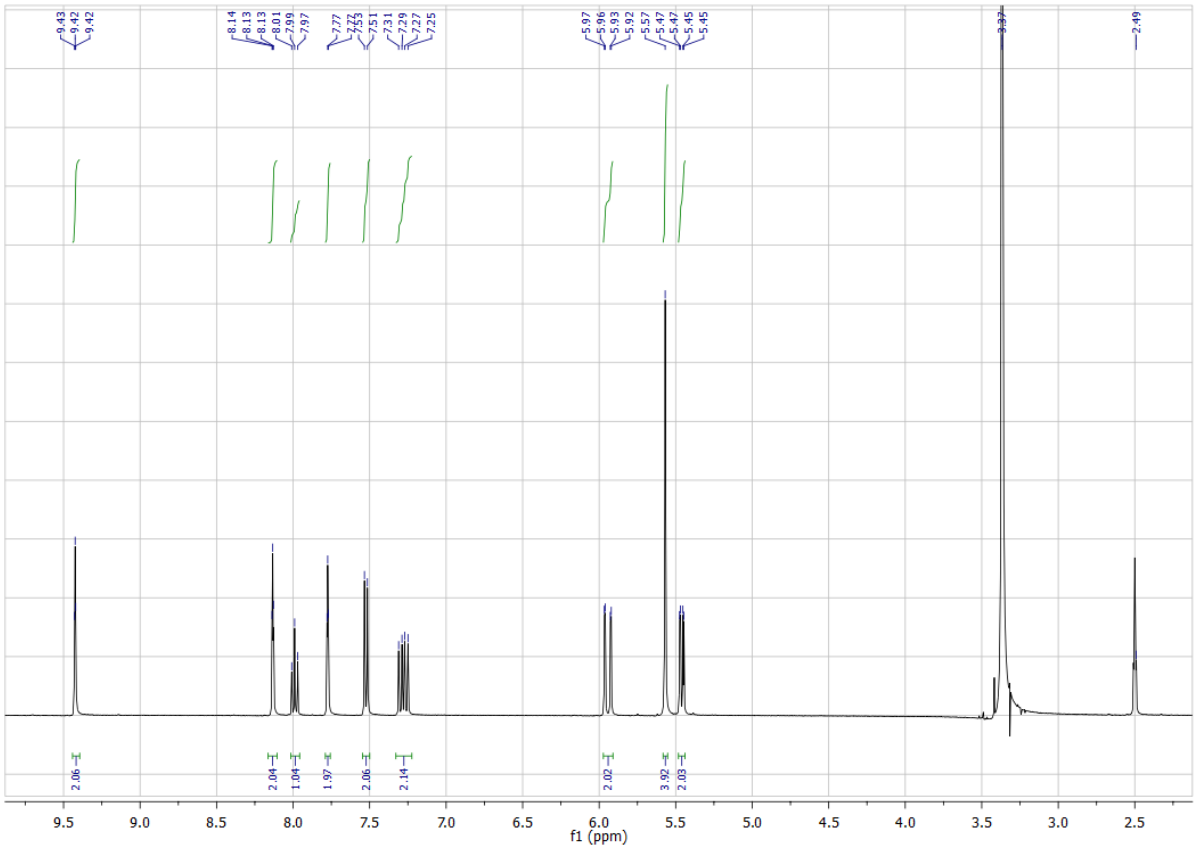

Fig. S33 ^{1}H NMR spectra of **bIm-PF$_6$** in DMSO-d$_6$ at 400 MHz (peak at 3.37 ppm is water).[29]

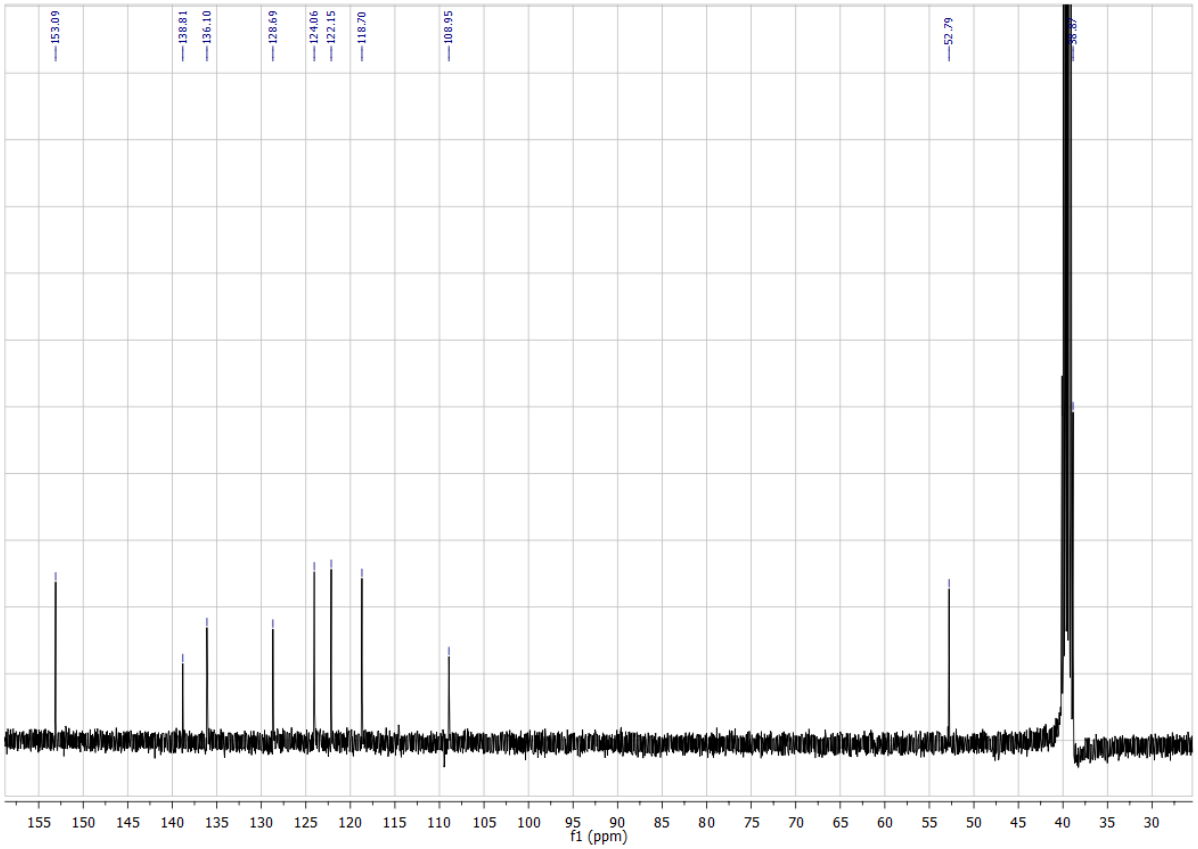

Fig. S34 ^{13}C NMR spectra of **bIm-PF$_6$** in DMSO-d$_6$ at 400 MHz.

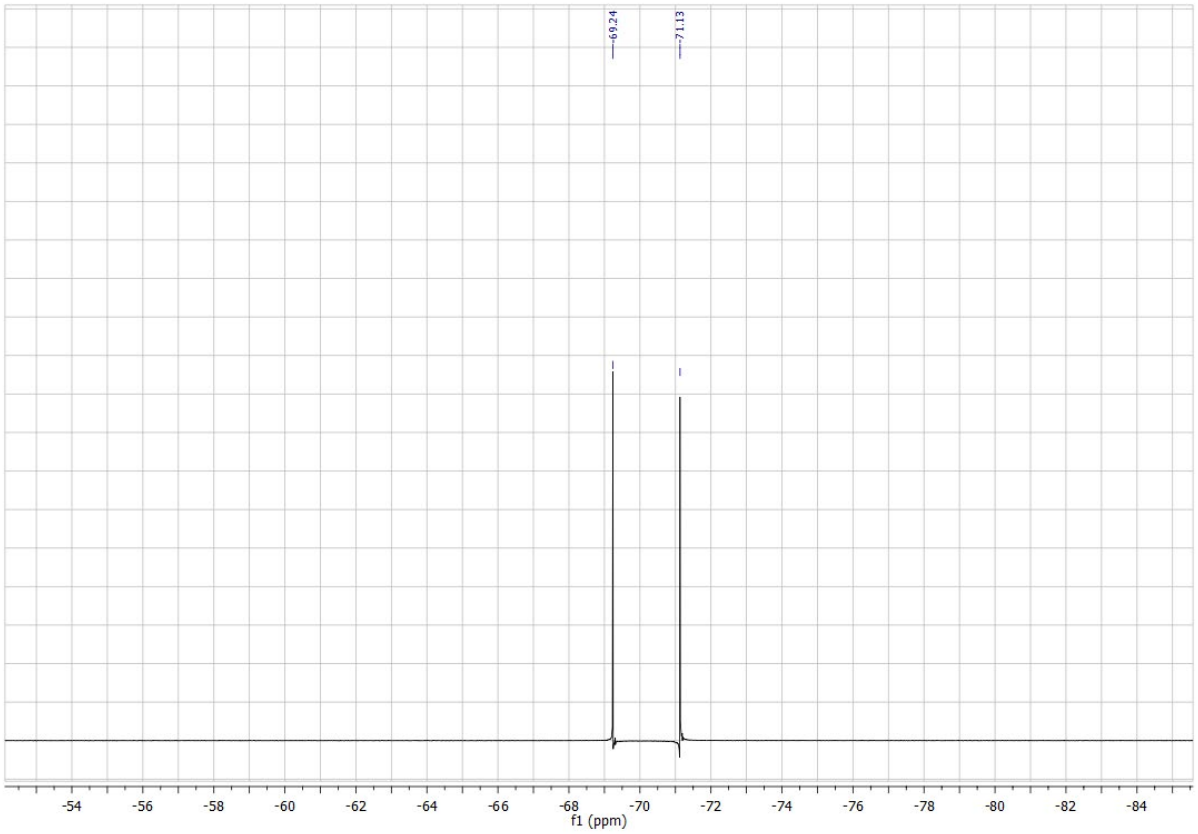

Fig. S35 ^{19}F NMR spectra of **bIm-PF$_6$** in DMSO-d$_6$ at 400 MHz.

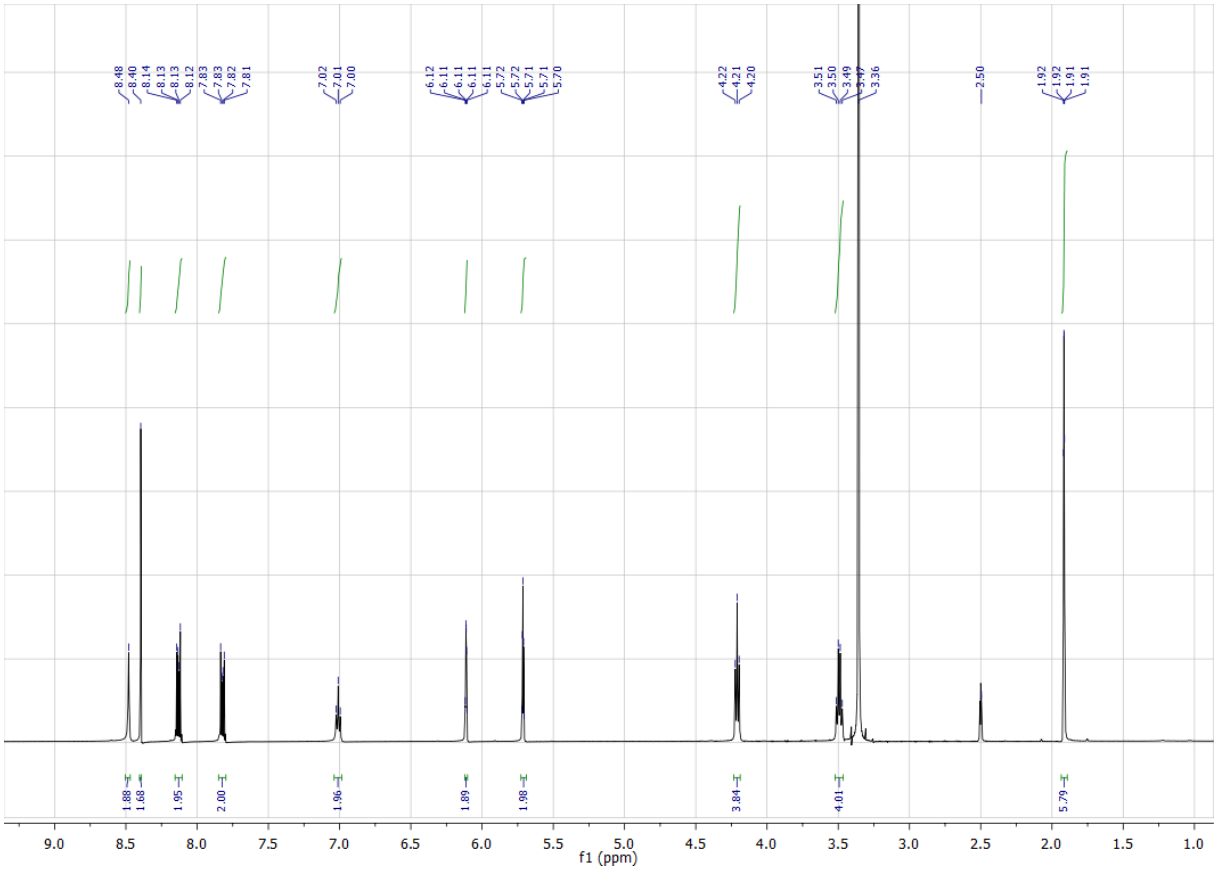

Fig. S36 ^{1}H NMR spectra of **fCL** in DMSO-d$_6$ at 400 MHz (peak at 3.36 ppm is water).[29]

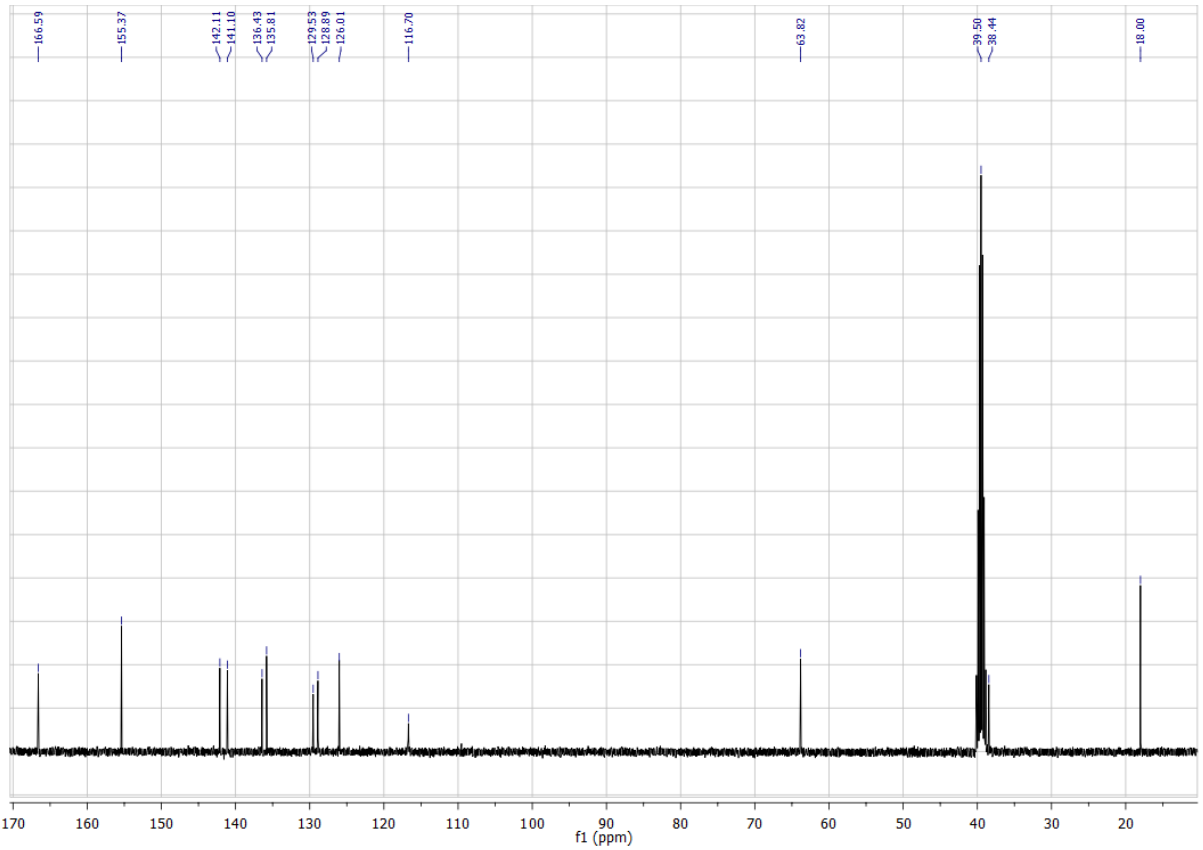

Fig. S37 ^{13}C NMR spectra of **fCL** in DMSO-d_6 at 400 MHz.

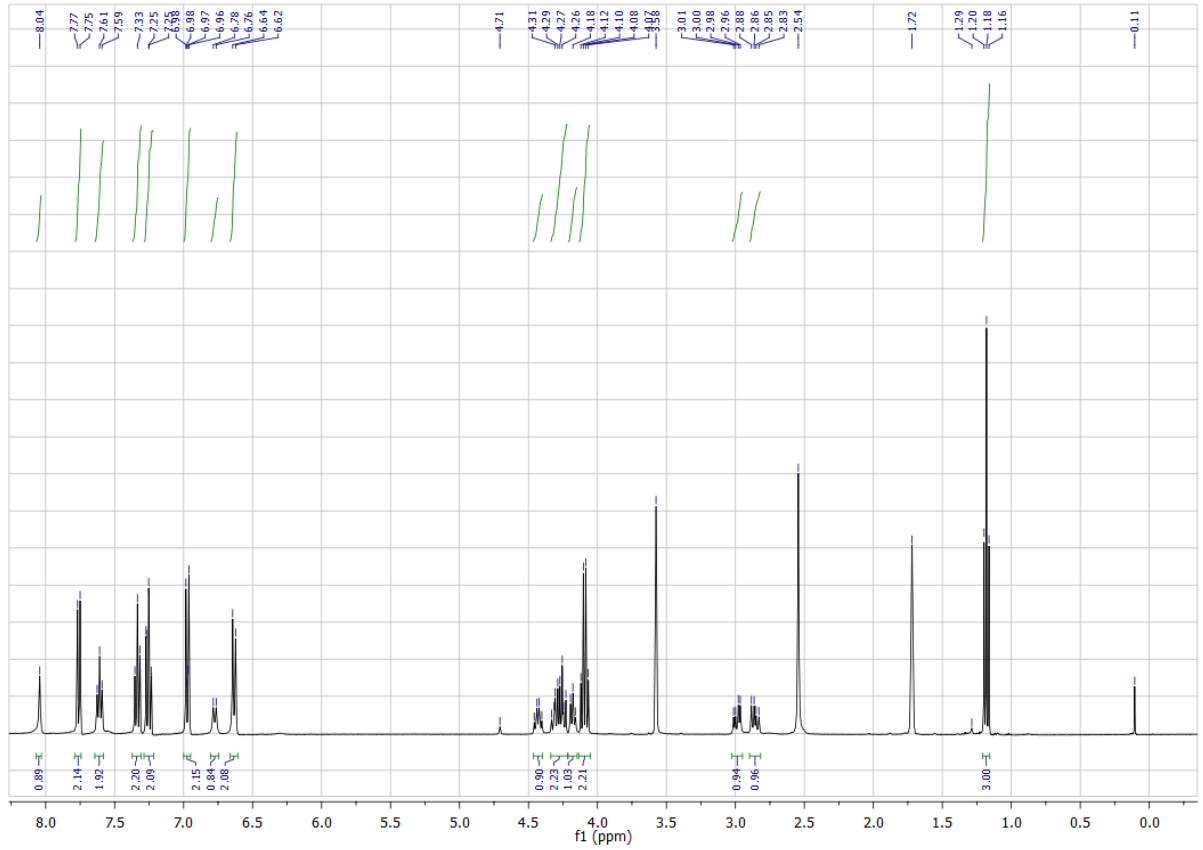

Fig. S38 ^{1}H NMR spectra of Fmoc-Y-OEt in THF-d_8 at 400 MHz (peak at 4.71 ppm is a minor impurity, 2.54 ppm is water, 1.29 ppm is H grease and 0.11 ppm is silicon grease).[29]

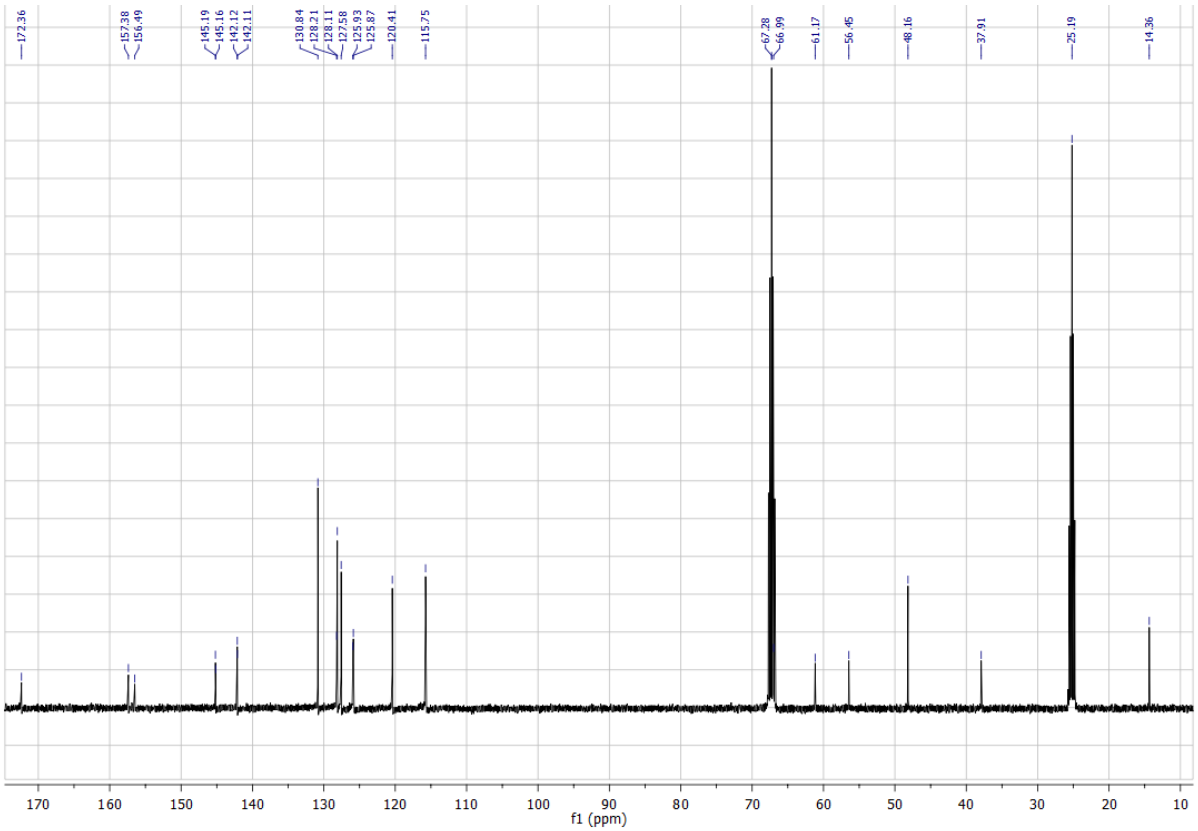

Fig. S39 ^{13}C NMR spectra of Fmoc-Y-OEt in THF-d_8 at 400 MHz.

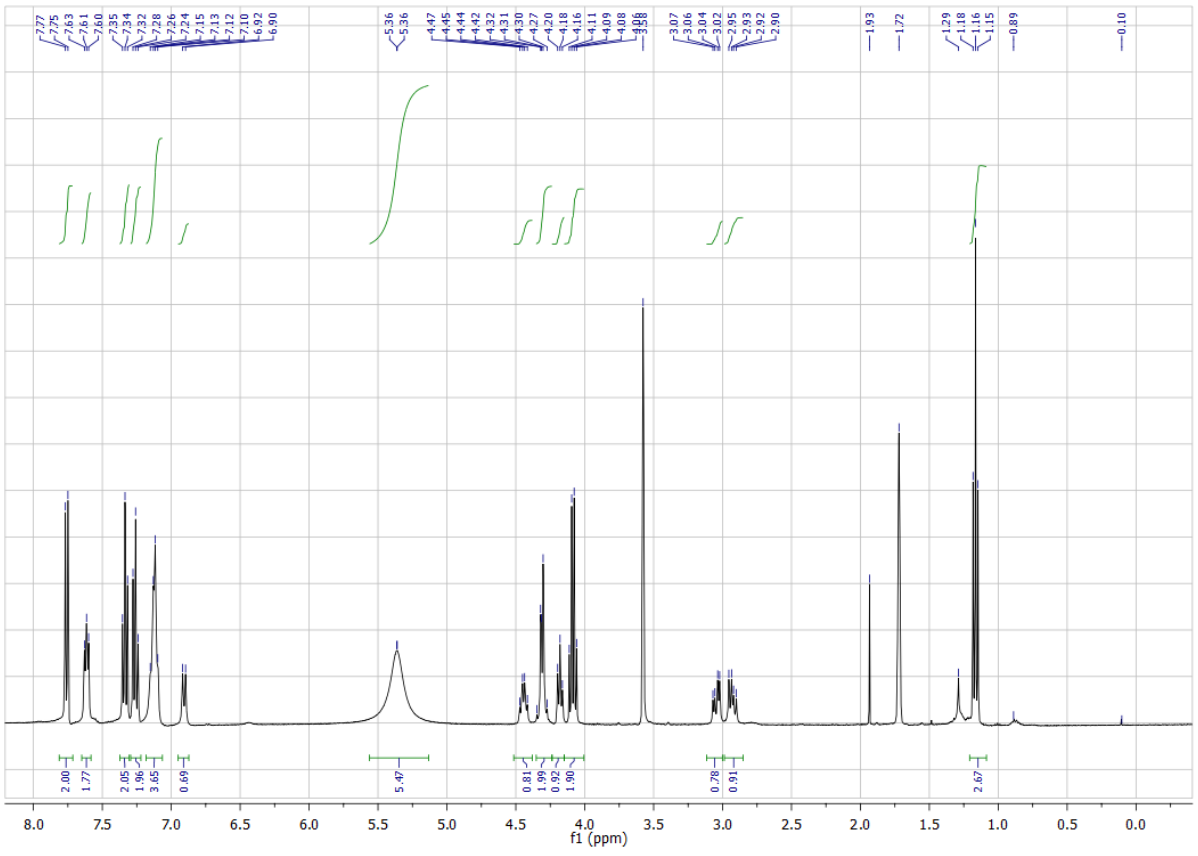

Fig. S40 ^{1}H NMR spectra of Fmoc-pY-OEt in THF-d_8 at 400 MHz (peak at 1.93 ppm is acetonitrile, 1.29 and 0.89 ppm is H grease and 0.10 ppm is silicon grease).[29]

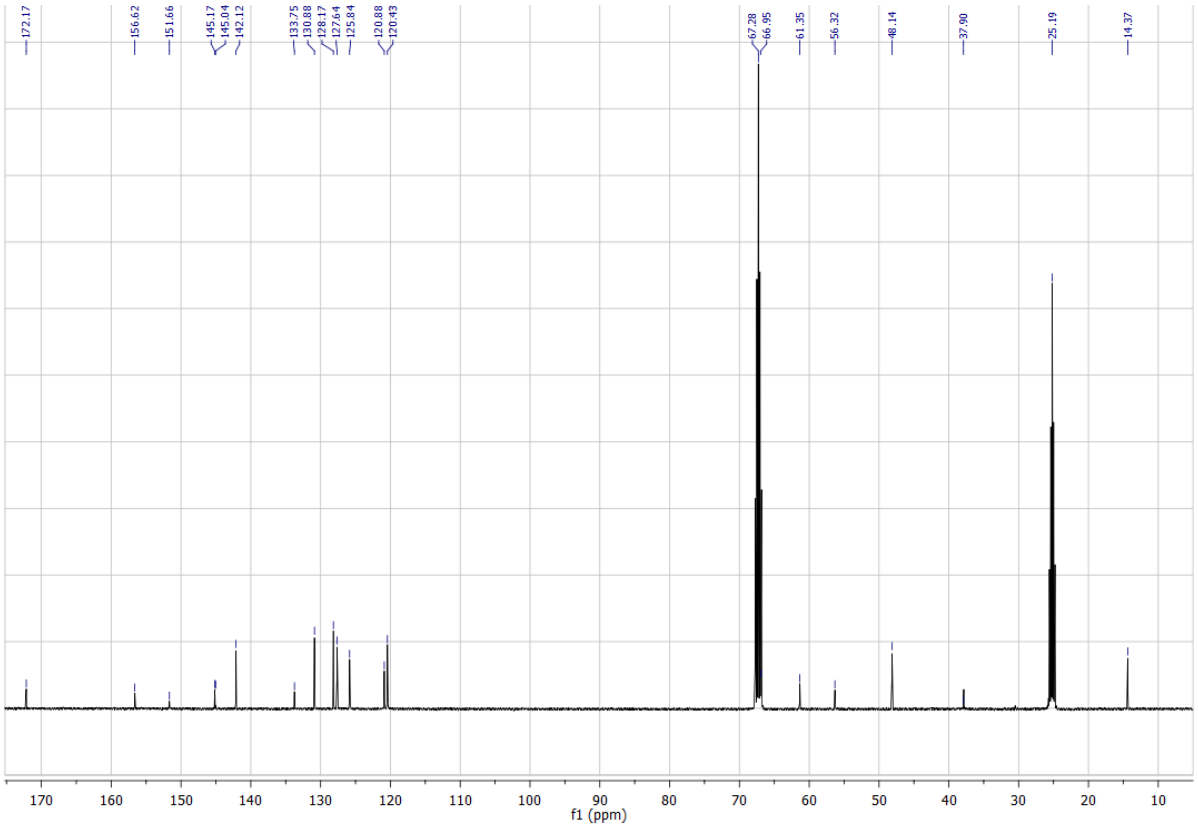

Fig. S41 ^{13}C NMR spectra of Fmoc-pY-OEt in THF-d_8 at 400 MHz.

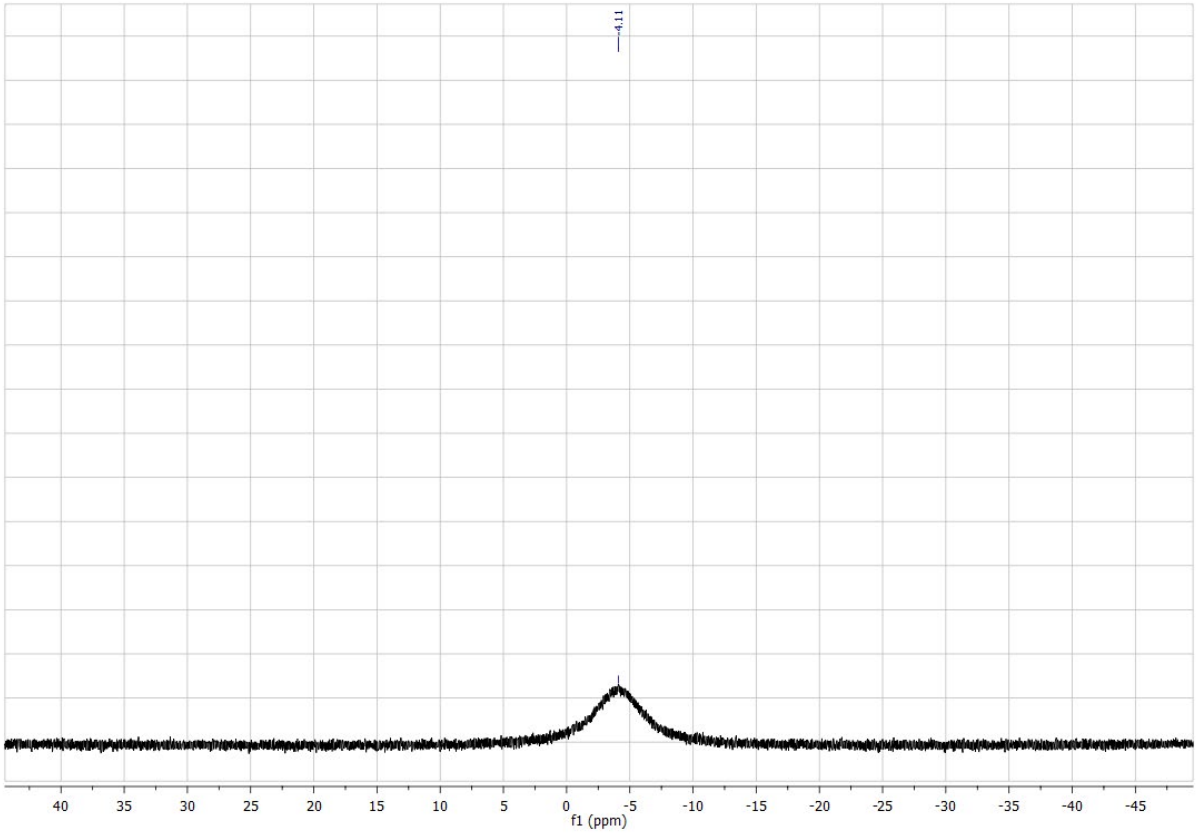

Fig. S42 ^{31}P NMR spectra of Fmoc-pY-OEt in THF-d_8 at 400 MHz.

References

1. P. Narayanaswamy, S. Shinde, R. Sulc, R. Kraut, G. Staples, C. H. Thiam, R. Grimm, B. Sellergren, F. Torta and M. R. Wenk, *Anal. Chem.*, 2014, **86**, 3043-3047.
2. O. Bakulina, F. K. Merkt, T. O. Knedel, C. Janiak and T. J. J. Muller, *Angew. Chem. Int. Ed.*, 2018, **57**, 17240-17244.
3. W. Wan, A. B. Descalzo, S. Shinde, H. Weißhoff, G. Orellana, B. Sellergren and K. Rurack, *Chem. Eur. J.*, 2017, **23**, 15974-15983.
4. C. Wierzbicka, M. Liu, D. Bauer, K. Irgum and B. Sellergren, *J. Mater. Chem. B*, 2017, **5**, 953-960.
5. S. Shinde, Z. El-Schich, A. Malakpour, W. Wan, N. Dizeyi, R. Mohammadi, K. Rurack, A. Gjoerloff Wingren and B. Sellergren, *J. Am. Chem. Soc.*, 2015, **137**, 13908-13912.
6. L. Munguia-Cortes, I. Perez-Hermosillo, R. Ojeda-Lopez, J. M. Esparza-Schulz, C. Felipe-Mendoza, A. Cervantes-Uribe and A. Dominguez-Ortiz, *J. Mex. Chem. Soc.*, 2017, **61**, 273-281.
7. E. Asenath Smith and W. Chen, *Langmuir*, 2008, **24**, 12405-12409.
8. R. A. Haque, S. F. Nasri, M. A. Iqbal, S. S. Al-Rawi, S. F. Jafari, M. B. K. Ahamed and A. M. S. Abdul Majid, *J. Chem.*, 2013, **2013**, 804683.
9. S. Chen, R. Vijayaraghavan, D. R. MacFarlane and E. I. Izgorodina, *J. Phys. Chem. B*, 2013, **117**, 3186-3197.
10. S. J. Pike, J. J. Hutchinson and C. A. Hunter, *J. Am. Chem. Soc.*, 2017, **139**, 6700-6706.
11. R. P. Matthews, I. J. Villar-Garcia, C. C. Weber, J. Griffith, F. Cameron, J. P. Hallett, P. A. Hunt and T. Welton, *Phys. Chem. Chem. Phys.*, 2016, **18**, 8608-8624.
12. ImageJ, https://imagej.nih.gov/ij/, (accessed November).
13. M. J. Frisch, G. W. Trucks, H. B. Schlegel, G. E. Scuseria, M. A. Robb, J. R. Cheeseman, G. Scalmani, V. Barone, G. A. Petersson, H. Nakatsuji, X. Li, M. Caricato, A. V. Marenich, J. Bloino, B. G. Janesko, R. Gomperts, B. Mennucci, H. P. Hratchian, J. V. Ortiz, A. F. Izmaylov, J. L. Sonnenberg, Williams, F. Ding, F. Lipparini, F. Egidi, J. Goings, B. Peng, A. Petrone, T. Henderson, D. Ranasinghe, V. G. Zakrzewski, J. Gao, N. Rega, G. Zheng, W. Liang, M. Hada, M. Ehara, K. Toyota, R. Fukuda, J. Hasegawa, M. Ishida, T. Nakajima, Y. Honda, O. Kitao, H. Nakai, T. Vreven, K. Throssell, J. A. Montgomery Jr., J. E. Peralta, F. Ogliaro, M. J. Bearpark, J. J. Heyd, E. N. Brothers, K. N. Kudin, V. N. Staroverov, T. A. Keith, R. Kobayashi, J. Normand, K. Raghavachari, A. P. Rendell, J. C. Burant, S. S. Iyengar, J. Tomasi, M. Cossi, J. M. Millam, M. Klene, C. Adamo, R. Cammi, J. W. Ochterski, R. L. Martin, K. Morokuma, O. Farkas, J. B. Foresman and D. J. Fox, *Journal*, 2016.
14. Bindfit, http://app.supramolecular.org/bindfit, (accessed November 2022).
15. D. Brynn Hibbert and P. Thordarson, *Chem. Commun.*, 2016, **52**, 12792-12805.
16. P. Thordarson, *Chem. Soc. Rev.*, 2011, **40**, 1305-1323.
17. V. A. Hackley and J. D. Clogston, *Special Publication (NIST SP)*, 2015, **1200-6**.
18. D. Wu, X. Guo, H. Sun and A. Navrotsky, *J. Phys. Chem. C*, 2015, **119**, 15428-15433.
19. T. M. Legge, A. T. Slark and S. Perrier, *J. Polym. Sci., Part A: Polym. Chem.*, 2006, **44**, 6980-6987.
20. Z. Duan, Z. Qu, F. Hu, Y. Yang, G. Chen and H. Xu, *Appl. Surf. Sci.*, 2014, **300**, 104-110.
21. K. Rurack and M. Spieles, *Anal. Chem.*, 2011, **83**, 1232-1242.
22. R. G. Pearson, *J. Am. Chem. Soc.*, 1963, **85**, 3533-3539.
23. S. Wagner, C. Zapata, W. Wan, K. Gawlitza, M. Weber and K. Rurack, *Langmuir*, 2018, **34**, 6963-6975.
24. K. Abraham, *J. Electrochem. Soc.*, 2014, **162**, A3021.
25. M. Maus and K. Rurack, *New J. Chem.*, 2000, **24**, 677-686.

26. A. Albert and J. N. Phillips, *J. Chem. Soc.*, 1956, 1294-1304.
27. D. A. Armbruster and T. Pry, *Clin. Biochem. Rev.*, 2008, **29 Suppl 1**, S49-S52.
28. *Evaluation of Measurement Data—Guide to the Expression of Uncertainty in Measurement*, Joint Committee for Guides in Metrology JCGM, Paris, 1 Edn , corrected version 2010 edn., 2008.
29. G. R. Fulmer, A. J. M. Miller, N. H. Sherden, H. E. Gottlieb, A. Nudelman, B. M. Stoltz, J. E. Bercaw and K. I. Goldberg, *Organometallics*, 2010, **29**, 2176-2179.